Transcriptional regulation of the Ciona Gsx gene in the neural plate

Clare Hudson, Rosaria Esposito, Antonio Palladino, Leopoldo Staiano, David E K Ferrier, Emmanuel Faure, Patrick Lemaire, Hitoyoshi Yasuo, Antonietta Spagnuolo

▶ **To cite this version:**

Clare Hudson, Rosaria Esposito, Antonio Palladino, Leopoldo Staiano, David E K Ferrier, et al.. Transcriptional regulation of the Ciona Gsx gene in the neural plate. Developmental Biology, 2019, 448 (2), pp.88-100. 10.1016/j.ydbio.2018.12.013 . hal-02115329

HAL Id: hal-02115329
https://hal.science/hal-02115329

Submitted on 22 Oct 2021

HAL is a multi-disciplinary open access archive for the deposit and dissemination of scientific research documents, whether they are published or not. The documents may come from teaching and research institutions in France or abroad, or from public or private research centers.

L'archive ouverte pluridisciplinaire **HAL**, est destinée au dépôt et à la diffusion de documents scientifiques de niveau recherche, publiés ou non, émanant des établissements d'enseignement et de recherche français ou étrangers, des laboratoires publics ou privés.

Distributed under a Creative Commons Attribution - NonCommercial - NoDerivatives 4.0 International License

Version of Record: https://www.sciencedirect.com/science/article/pii/S0012160618303853
Manuscript_e12ed3efd44d3227e950dfea67783f06

Transcriptional regulation of the *Ciona Gsx* gene in the neural plate

Clare Hudson[1*$], Rosaria Esposito[2,3$], Antonio Palladino[2-9], Leopoldo Staiano[2,8], David Ferrier[4], Emmanuel Faure[5,6], Patrick Lemaire[7], Hitoyoshi Yasuo[1] and Antonietta Spagnuolo[2*$]

***corresponding authors**
$ equal contributors

1- Sorbonne Université, CNRS, Laboratoire de Biologie du Développement de Villefranche-sur-mer (LBDV), 06230 Villefranche-sur-mer, France
2- Biology and Evolution of Marine Organisms, Stazione Zoologica Anton Dohrn, Napoli 80121, Italy
3- Current address: Enzo Life Sciences 13, avenue Albert Einstein, 69100 Villeurbanne, France
4- The Scottish Oceans Institute, Gatty Marine Laboratory, University of St Andrews, East Sands, St Andrews, KY16 8LB, UK
5- Institut de Biologie Computationnelle, Université de Montpellier, Montpellier, France
6- Team VORTEX, Institut de Recherche en Informatique de Toulouse, Universities Toulouse I and III, CNRS, INPT, ENSEEIHT; 2 rue Camichel, BP 7122, F-31071 Toulouse Cedex 7, France
7- CRBM, Université de Montpellier, France
8- Current address: Tigem (Telethon Institute of Genetics And Medicine), Via Campi Flegrei, 34, 80078 Pozzuoli Napoli, Italy
9- Current address: Center for Advanced Biomaterials for Health Care/CRIB, Largo Barsanti e Matteucci 53 80125 Napoli, Italy

© 2018 published by Elsevier. This manuscript is made available under the CC BY NC user license
https://creativecommons.org/licenses/by-nc/4.0/

ABSTRACT

The ascidian neural plate consists of a defined number of identifiable cells organized in a grid of rows and columns, representing a useful model to investigate the molecular mechanisms controlling neural patterning in chordates. Distinct anterior brain lineages are specified via unique combinatorial inputs of signalling pathways with Nodal and Delta-Notch signals patterning along the medial-lateral axis and FGF/MEK/ERK signals patterning along the anterior-posterior axis of the neural plate. The *Ciona Gsx* gene is specifically expressed in the a9.33 cells in the row III/column 2 position of anterior brain lineages, characterised by a combinatorial input of Nodal-OFF, Notch-ON and FGF-ON. Here, we identify the minimal cis-regulatory element (CRE) of 376bp, which can recapitulate the early activation of *Gsx*. We show that this minimal CRE responds in the same way as the endogenous *Gsx* gene to manipulation of FGF- and Notch-signalling pathways and to overexpression of Snail, a mediator of Nodal signals, and Six3/6, which is required to demarcate the anterior boundary of *Gsx* expression at the late neurula stage. We reveal that sequences proximal to the transcription start site include a temporal regulatory element required for the precise transcriptional onset of gene expression. We conclude that sufficient spatial and temporal information for *Gsx* expression is integrated in 376bp of non-coding cis-regulatory sequences.

Keywords: ascidian, Ciona, Gsx, transcriptional regulation, promoter, neural patterning, para-hox

INTRODUCTION

The swimming larva of ascidians (Tunicata) possesses a distinctive chordate body plan featuring a central notochord with an overlying central nervous system (CNS). Its tripartite CNS forms by neurulation and is made up of an anterior sensory vesicle, a trunk ganglion and a caudal nerve cord. Overall, it contains around 330 cells, two thirds of which are within the sensory vesicle, thus forming one of the simplest chordate larval nervous systems (Cole and Meinertzhagen, 2004; Meinertzhagen et al., 2004).

What makes ascidian embryos so appealing is that CNS formation proceeds with a restricted number of identifiable cells, whose invariant cell lineages and fate maps are well documented (Cole and Meinertzhagen, 2004; Nicol and Meinertzhagen, 1988; Nishida, 1987) (reviewed in (Hudson, 2016)). Each neural plate cell is produced by a series of stereotypical divisions, has its own specific identity and can be easily recognized, thus permitting a level of accuracy not currently applicable to any other chordate model (Cole and Meinertzhagen, 2004; Navarrete and Levine, 2016; Nicol and Meinertzhagen, 1988; Nishida, 1987).

At the 8-cell stage, four founder lineages are born: the a- and b- animal lineages and the A- and B- vegetal lineages. Three of these lineages, A-, a- and b-, contribute to the CNS. At neural plate stage, cells are aligned in a grid-like organization, such that at the late gastrula stage (stage 12 or '6-row stage' (Hotta et al., 2007)), the neural plate consists of six rows and eight columns of regularly aligned cells (Figure 1, top right). Along the anterior-posterior axis, the posterior-most two rows (I-II) of the neural plate are of A-lineage origin and generate the posterior part of the sensory vesicle as well as the ventral and lateral trunk ganglion and tail nerve cord. The anterior four rows (III-VI) are of a-lineage origin. Of these, only rows III and IV contribute to the CNS, generating the anterior part of the sensory vesicle, the ascidian 'brain', as well as contributing to the oral siphon (Cole and Meinertzhagen, 2004; Nishida, 1987; Taniguchi and Nishida, 2004; Veeman et al., 2010). Along the medial-lateral axis, cells are arranged in four bilateral pairs of columns. Column 1 is the medial most pair of columns, and the lateral-most column is column 3 for the anterior a-lineage derived part of the neural plate and column 4 for the posterior A-lineage derived part of the neural plate. Several b-lineage cells bordering the neural plate generate the dorsal roof of the neural tube.

The molecular events leading to individual cell specification have also been studied in detail (reviewed in (Hudson, 2016)). Unique molecular signatures, characterized by specific combinations of gene expression, have been described for most neural plate cells. A particular combinatorial action of three signalling pathways, Nodal, Delta2/Notch and FGF/MEK/ERK, defines each of the distinct cell identities that make up rows I and II of the neural plate (Hudson et al., 2007; Hudson

and Yasuo, 2005; Imai et al., 2006; Mita and Fujiwara, 2007). More recently, it has been shown that very similar molecular mechanisms also operate during patterning of the row III anterior brain precursors of the neural plate. These studies indicate that, like in the A-lineage derived neural plate, Nodal and Delta-Notch are involved in medio-lateral patterning, while FGF/MEK/ERK signalling is required for anterior-posterior patterning of the a-lineage derived neural plate (Esposito et al., 2017; Haupaix et al., 2014; Racioppi et al., 2014).

In this study, we aimed to address how these patterning mechanisms lead to specific gene activation. To this end, we focused on the *Gsx* gene, which is specifically activated in the a9.33 cell pair, residing in the row III/column 2 position of anterior sensory vesicle lineages at the 6-row neural plate stage (Figure 1). *Gsx* expression is maintained in both daughter cells of a9.33 (a10.66 and a10.65) at the neurula stage, when additional expression is also observed in medial (column 1) cells (a10.73) (Figure 1). By the late neurula and early tailbud stages, expression is also observed in posterior sensory vesicle precursors of A-lineage origin. We present our analysis of the cis-regulatory sequences that can recapitulate early activation of the *Ciona Gsx* gene. We identified a 376bp minimal element required for the activation of *Gsx* in the a9.33 pairs and their progeny at the neurula stage. Our analysis suggests that the fine spatial and temporal regulation of *Gsx* expression involves activating MEK/ERK and Notch, and repressing Snail and Six3/6 regulatory inputs.

RESULTS

Isolation of the *Gsx* regulatory region

In this study, we indiscriminately used two very similar ascidian species for our electroporation assays, *Ciona robusta* and *Ciona intestinalis* (formerly *Ciona intestinalis* types *A* and *B* respectively). At the late gastrula stage (stage 12, approximately 6.5 hours of development at 18°C; Figure 1, top), the embryo has a neural plate made of 6-rows of cells called, from posterior to anterior, row I to VI. At the mid-neurula stage (stage 15, approximately 8 hours of development at 18°C; Figure 1, second row), row III cells have divided into row IIIa (anterior) and row IIIp (posterior) (Hotta et al., 2007).

The precise and specific activation of *Gsx* in the a9.33 pair of cells in row III at the neural plate stage prompted us to explore the mechanisms involved in its transcriptional regulation. A genomic fragment of about 3.9 kb (-3857 to +11 of the first base of the KH2012:KH.C2.917 transcript model (Satou et al., 2008) was cloned from a *Ciona robusta* cosmid library and placed upstream of *LacZ* (*pGsx[-3857,+11]>LacZ*). Electroporation of this plasmid DNA revealed that the 3.9kb region was sufficient to recapitulate endogenous *Gsx* expression from the neural plate stage

(Figure 1). *LacZ* reporter gene expression could be detected by *in situ* hybridisation in the a9.33 pair of cells. At neurula stage, like endogenous *Gsx, pGsx[-3857,+11]*-driven *LacZ* expression was detected in medial row III cells as well as the a9.33 daughters. *pGsx[-3857,+11]*-driven *LacZ* expression continues to mirror endogenous *Gsx* gene expression at the late neurula and early tailbud stages, with expression expanding posteriorly into the A-line-derived posterior sensory vesicle precursors at these stages (Figure 1). Using detection of β-galactosidase enzymatic activity, a much simpler assay, we obtained similar results, but with a time delay in the onset of detection, presumably due to the time taken to translate a sufficient level of β-galactosidase protein. β-galactosidase enzymatic activity could be detected from the neurula stage, when a9.33 has divided into a10.66 and a10.65. In the following studies, we chose to focus on the simpler β-galactosidase activity assay at the neurula stage, as a proxy for gene activation at the neural plate stage.

We set out to identify the minimal cis-regulatory element that was sufficient to drive neurula stage β-galactosidase activity in the a9.33 daughters. We conducted a 5' deletion analysis of *pGsx[-3857, +11]* to generate *pGsx[-1905, +11]*, *pGsx[-829, +11]*, *pGsx[-636, +11]*, *pGsx[-365, +11]*, *pGsx[-297, +11]*, *pGsx[-256, +11]*, *pGsx[-193, +11]*, *pGsx[-120, +11]* (Figure 2). Constructs *pGsx[-1905, +11]* to *pGsx[-256, +11]* drove β-galactosidase activity in the a9.33 daughters, often with reduced activity compared to the *pGsx[-3857, +11]* construct, whereas the *pGsx[-193, +11]* and *pGsx[-120 +11]* constructs did not drive a detectable level of β-galactosidase activity (Figure 2). This suggests that critical cis-regulatory elements required to drive neural plate expression are present between positions -256 and -193bp upstream of the transcription start site. Consistent with this idea, removing the -278- to -121 sequences from the *pGsx[-3857, +11]* construct (*pGsx[-3857, -279][-120, +11])* resulted in the loss of transgene activity (Supplementary Figure 1).

Focusing on the sequences around the [-256, -193] domain, we carried out various overlapping window deletions in order to further define the essential elements for correct neural plate expression (Figure 3A). Individual fragments were cloned upstream of the *Brachyury* minimal promoter (*bpBra*) (Bertrand et al., 2003). Ectopic "mesenchyme" (mesenchyme plus additional unidentified internal cells) activity was frequently observed when using *bpBra*. Neural expression, however, was never observed with *bpBra* alone (3 independent experiments, total n= 952). Hence, for the following analysis, only neural expression was considered (Figure 3B). The constructs *pGsx[-297, -100]bpBra, pGsx[-297, -176]bpBra, pGsx[-256, -100]bpBra* and *pGsx[-365, -236]bpBra* exhibited β-galactosidase activity at the neurula stage, whereas constructs *pGsx[-256, -176]bpBra, pGsx[-297, -236]bpBra* and *pGsx[-193, -100]bpBra* drove very weak or no β-galactosidase activity (Figure 3B). As *pGsx[-365, -236]bpBra* and *pGsx[-256, -100]bpBra* are both active, despite a very small region of overlap, this suggests the presence of multiple positive inputs.

In support of the idea that no single region of the upstream sequences is critical for activation in neural cells, a systematic 20bp window deletion analysis between the -256 to -100 regions of the *pGsx[-297, -100]bpBra* construct did not result in loss of transgene activity (Supplementary Figure 2).

Interestingly, this analysis also suggested that there may be some negative control elements located in the part of the sequence closest to the transcription start site. Electroporation of constructs lacking these elements resulted in lateral (column 3, green in Figure 3B-C) and/or anterior (into row IV precursors, blue in Figure 3B-C) ectopic expansion of β-galactosidase staining. The *pGsx[-365, -236]bpBra* construct gave a particularly striking increase in anterior expansion into row IV cells (Figure 3B lower graph, C). The smaller fragment constructs (*pGsx[-297, -236]bpBra* and *pGsx[-256, -176]bpBra*) only drove very weak neural expression, making any conclusion on ectopic activity difficult (Figure 3B).

In conclusion, partial deletions around the [-256, -193] sequences identify two types of regulatory inputs. Since the *pGsx[-365, -236]bpBra* and *pGsx[-256, -100]bpBra* constructs were both active, we conclude that the -365 to -100 sequences mediate multiple positive inputs with no single region essential for neural expression (Figure 3; Supplementary Figure 2). The -235 to +11 sequences likely contains repressive elements, which act to restrict *Gsx* expression to row III and column 2 (Figure 3). Thus, we consider that the entire -365 to +11 sequences contain important elements to drive accurate expression of *Gsx* in the neural plate of wild-type embryos and used the *pGsx[-365+11]* construct for subsequent experiments.

Evidence for a FGF/MEK/Ets-Elk signalling response elements in the -365 to +11 regulatory sequences

Focusing on the [-365, +11] sequences identified above, we next tested whether experimental manipulations affecting endogenous *Gsx* expression similarly affect reporter gene expression driven by *pGsx[-365, +11]*. In *Ciona*, FGF-ERK signalling is essential for both the initial neural induction at the 32-cell stage (Bertrand et al., 2003; Hudson et al., 2003) and the subsequent anterior-posterior patterning of the CNS (Haupaix et al., 2014; Hudson et al., 2007; Racioppi et al., 2014; Wagner and Levine, 2012). In particular, differential activation of FGF/ERK signals between rows III and IV takes place, with ERK active in row III cells where it promotes row III gene expression and represses row IV gene expression (Haupaix et al., 2014; Racioppi et al., 2014). This signalling pathway could thus be required for *Gsx* expression.

To confirm this, we treated embryos from the early gastrula stage with the pharmacological agent U0126, an inhibitor of the MAP kinase kinase, MEK1/2. This resulted in a strong reduction in

Gsx expression (Figure 4A). We next tested whether the *pGsx[-365, +11]* construct contained a MEK-ERK response element by treating embryos electroporated with this construct with U0126 at the early gastrula stage. Similar to endogenous *Gsx* expression, transgene activity driven by *pGsx[-365, +11]* was completely suppressed by U0126 treatment (Figure 4B).

Several recent studies show that, during *Ciona* embryogenesis, members of the ETS family of transcription factors (Ets1/2 and Elk1/3/4) act as downstream effectors of FGF/ERK signalling (Bertrand et al., 2003; Davidson et al., 2006; Gainous et al., 2015; Squarzoni et al., 2011). To investigate the role of Ets/Elk in *Gsx* gene activation, we expressed constitutive repressor or activator forms of Ets1/2 (Ets:WRPW and Ets:VP16, respectively) or Elk1/3/4 (Elk:WRPW and Elk:VP64, respectively) throughout the neural plate using the *Zic-r.b* promoter, which is active in the a-neural lineages at the 6-row neural plate stage (Abitua et al., 2012; Gainous et al., 2015; Wagner and Levine, 2012). Expression of repressor forms of both Elk and Ets led to a reduction of endogenous *Gsx* expression (Figure 4C, F). By contrast, overexpression of activator forms did not affect the spatial pattern of *Gsx* expression. Overexpression of Ets and Elk fusion proteins had a similar effect on the ß-galactosidase activity driven by *pGsx[-365, +11]* (Figure 4D, E).

Taken together, these data show that Ets family transcription factors, most likely mediating FGF/MEK/ERK signals, are required for *Gsx* gene activation and that the *Gsx* [-365 to +11] sequences contain elements mediating this activation. Consistent with this idea, bioinformatic analyses of these sequences revealed several potential Ets family transcription factor binding sites (Supplementary Figure 3). We conclude that the *Gsx* gene is most likely activated directly by the FGF/MEK/ERK signalling pathway in row III via Ets family members.

Evidence for Delta/Notch response elements in the -365 to +11 regulatory sequences

Previous data show that Delta-Notch signalling is required to promote *Gsx* expression in column 2 of the ascidian neural plate (Esposito et al., 2017). Inhibition of the Notch signalling pathway resulted in a strong reduction of *Gsx* expression, whereas overexpression of *Delta-like* had the opposite effect, promoting ectopic *Gsx* expression in column 1 cells. In order to test whether the [-365, +11] sequences contained a Notch response element, we treated *pGsx[-365, +11]* electroporated embryos with DAPT (an inhibitor of gamma-secretase, which is required for Notch receptor processing) to block the pathway. Treatment of embryos with DAPT from the early gastrula stage resulted in reduction of neural β-galactosidase activity (Figure 5A). We conclude that the *Gsx* -365 to +11 sequences contain the information necessary to respond to Notch signalling. While our bioinformatic analysis revealed a site at -205 with a perfect match to the consensus binding site of Su(H) (TGGGAA, on the reverse strand), the transcription factor that mediates

Notch signalling (Fortini and Artavanis-Tsakonas, 1994), removal of this sequence in the deletion construct D3 did not result in loss of neural activity of the construct, suggesting that this binding site is not critical (Supplementary Figure 2).

Evidence for a Snail response element in the 365 to +11 regulatory sequences

We recently showed that the transcription factor Snail (Nieto, 2002) is involved in the repression of *Gsx* in column 3 cells at the 6-row neural plate stage (Esposito et al., 2017). Like endogenous *Gsx*, β-galactosidase activity driven by *pGsx[-365, +11]* was strongly reduced when co-electroporated with *pEtr>Snail* (Figure 5B), suggesting that elements responsible for Snail-mediated repression are present within the -365 to +11 sequences. Indeed, a bioinformatic search for potential Snail binding sites conserved between *Ciona robusta* and *Ciona savigni* (Supplementary Figure 3), as well as a ChIP-chip analysis of Snail (Kubo et al., 2010) suggests that Snail may interact directly with the *Gsx* upstream sequences. Interestingly, the predicted binding site with highest affinity for Snail maps close to the TSS around -11, which is removed in *pGsx[-297, -100]bpBra*, a construct driving lateral expansion of β-galactosidase activity (Figure 3).

Evidence for Six response elements in the -365 to +11 regulatory sequences

In the previous section, we showed that removal of the [-235, +11] sequences in *pGsx[-365, -236]bpBra* resulted in anterior expansion of β-galactosidase activity to row IV (Figure 3). One potential explanation for this observation is the presence of a repressor in row IV cells that interacts with sequences within the [-235, +11] region. The Six family members of homeodomain transcription factors can form composite transcription factors that can activate or repress transcription of downstream targets depending on the cellular context (Kumar, 2009). *Six3/6* is the single *Ciona* orthologue of *Six3* and *Six6* paralogues of vertebrate Six genes (Wada et al., 2003). *Six3/6* is a very good candidate to repress *Gsx* expression in row IV as it is specifically expressed in row IV cells from the 6-row neural plate stage, just anterior to endogenous *Gsx* expression (Imai et al., 2004). The two other *Ciona* Six gene class members, *Six1/2* and *Six4/5*, are not expressed in row IV cells (Imai et al, 2004). In order to address if Six3/6 might play a role in *Gsx* gene regulation, we first tested whether Six3/6 overexpression could repress endogenous *Gsx* expression. We overexpressed *Six3/6* throughout the neural plate from the early gastrula stage, using *pEtr>Six3/6*. This resulted in downregulation of *Gsx* expression at the neurula stage, suggesting a potential link between *Six3/6* and *Gsx* (Figure 6A). In contrast, morpholino (MO)-mediated knockdown of Six3/6 resulted in ectopic *Gsx* expression in row IV cells at the late neurula stage (Figure 6C). We used two different morpholino oligonucleotides designed to block translation, both of which generated

the same phenotype (Figure 6C; Supplementary Figure 4A). We also confirmed that both MOs successfully blocked translation of a reporter gene with corresponding target sequences by injecting each MO with the *Six3/6* upstream regulatory sequences driving *Venus* (*pSix3/6>Venus*). While YFP protein was detected in the anterior CNS of larvae injected with *pSix3/6>Venus* alone, co-injection of *pSix3/6>Venus* with either Six3/6-MO resulted in strong reduction of YFP protein levels (Supplementary Figure 4B). Thus, overexpression of *Six3/6* results in repression of *Gsx*, whereas inhibition of *Six3/6* results in ectopic expression of *Gsx* in row IV cells.

We next tested whether the [-365, +11] sequences contained a Six3/6-response element. Co-electroporation of *pGsx[-365, +11]>LacZ* with *pEtr>Six3/6* caused a strong decrease of β-galactosidase activity at the neurula stage, suggesting that the [-365, +11] sequences may contain binding sites for Six3/6 (Figure 6B). In support of a direct role for Six3/6 in *Gsx* repression in anterior neural cells, we found multiple predicted Six transcription factor binding sites within the [-365, +11] sequences (Supplementary Figure 3).

Finally, we tested the hypothesis that the [-235, +11] sequences, removed in *pGsx[-365, -236]bpBra*, were acting as a Six3/6-response element. In other words, whether removal of this potential Six response element was the reason that ectopic anterior transgene activity was observed with the *pGsx[-365, -236]bpBra* construct. If these sequences acted as the Six3/6 response element, then we predicted that removal of them would render the construct insensitive to Six3/6 overexpression. However, this was not the case, co-electroporation of *pEtr>Six3/6* and *pGsx[-365, -236]bpBra* revealed that Six3/6 was still able to strongly suppress the transgene activity, suggesting that the [-235, +11] sequences are not acting as the sole Six3/6-response element (Figure 6D).

Evidence for a temporal response element in the -235 to +11 regulatory sequences

Both FGF and Notch signals are required for *Gsx* expression in a9.33 cells at the neural plate stage. However, these signals are both present at earlier stages of development. *Delta-like* is expressed in lateral b- and A-line neural precursors adjacent to the a-line neural precursors from the 64-cell stage (Esposito et al., 2017; Hudson et al., 2007) and ERK1/2 is active in row III/IV mother cells at the early gastrula stage (Nishida, 2003; Wagner and Levine, 2012; Yasuo and Hudson, 2007). However, *Gsx* is not activated at this earlier stage, suggesting the presence of a temporal control mechanism.

To identify the cis-regulatory sequences preventing the precocious activation of *Gsx*, we collected embryos electroporated with either *pGsx[-365, -236]bpBra* or *pGsx[-365, +11]* every 30 minutes (at 18°C) from the 6-row neural plate stage. We observed neural β-galactosidase activity in *pGsx[-365, -236]bpBra* embryos at least 30 minutes before we observed any β-galactosidase

activity in *pGsx[-365, +11]* embryos (Figure 7). Taking into account the time-lag of LacZ detection (Figure 1), we consider that *pGsx[-365, -236]bpBra* therefore becomes active prior to the 6-row neural plate stage, thus in the row-III/IV mother cells. Consistently, *pGsx[-365, -236]bpBra*-electroporated embryos displayed clear ectopic β-galactosidase staining in cells in row IV and column 3 (Figure 7). This suggests that the ectopic activity observed in row IV with *pGsx[-365, -236]bpBra* is, at least in part, due to the precocious activation of the transgene in the precursor of both rows III and IV and that the [-235, +11] sequences include a temporal control element ensuring the delayed activation of *Gsx* solely in row III.

DISCUSSION

It was previously shown that medial-lateral patterning across the developing neural plate, triggered by Nodal, is required for the expression of *Gsx* in column 2 cells of the neural plate (Esposito et al., 2017). Nodal is involved both in promoting *Gsx* expression in column 2, via the activation of Delta-Notch signalling, and inhibiting *Gsx* expression in column 3, via the activation of the *Snail* repressor. It was also described that differential activation of the ERK signalling pathway patterns sibling neural plate cells along the anterior-posterior axis, with its role in *Gsx* regulation confirmed in this study (Figure 4) (Gainous et al., 2015; Haupaix et al., 2014; Hudson et al., 2007; Racioppi et al., 2014; Squarzoni et al., 2011). Here, we reveal a role for Six3/6 in restricting *Gsx* expression to row-III precursors at the late neurula stage (Figure 6).

In this study, we analysed the cis-regulatory sequences driving *Gsx* expression in the neural plate (Figure 8). We identified a -365 to +11 minimal promoter element, which recapitulated endogenous *Gsx* expression in the neural plate and responded, as endogenous *Gsx*, to manipulation of MEK-ERK-Ets signalling, Notch-signalling and Snail or Six3/6 overexpression. Our extensive deletion analysis of a [-365, +11] minimal promoter indicated that *Gsx* regulation is likely to be complex and modular, with no single region essential. This suggests redundancy between individual transcription factor binding sites, as was described for *Halocynthia Otx* cis-regulation (Oda-Ishii et al., 2005). The deletion analysis revealed the importance of sequences close to the transcriptional start site in limiting expression to the correct cells, including an element mediating temporal control (Figure 8).

Activation mechanisms for *Gsx* expression

In the neural plate, Nodal induces column 2 gene expression most likely indirectly, via activating gene expression of a Delta ligand (Esposito et al., 2017; Hudson et al., 2007). We were able to show that the [-365, +11] minimal promoter of *Gsx* contained a Notch response element. A potential

Su(H) consensus binding site was found in these sequences at position -205, although this did not appear to be essential for transgene activation (Supplementary Figure 2). This may indicate that Notch signalling is acting indirectly on the [-365, +11] minimal promoter of *Gsx*.

The other major positive input for *Gsx* expression is likely to be the Fibroblast Growth Factor (FGF) signalling pathway. This signalling pathway is used repeatedly following anterior-posterior cell divisions to specify posterior over anterior cell identities in the developing CNS (Haupaix et al., 2014; Hudson et al., 2007; Racioppi et al., 2014; Squarzoni et al., 2011; Wagner and Levine, 2012). In particular, differential activation of ERK1/2 occurs between a-line sister rows III and IV, with ERK1/2 activated in row III and inactive in row IV. This activation of ERK1/2 was shown to be required for specification of the a9.49 pair of cells in column 3 of row III and is then repeatedly required, following each anterior-posterior oriented cell division, in order for this lineage to eventually give rise to the pigmented cells of the ocellus and otolith in the brain (Haupaix et al., 2014; Racioppi et al., 2014). Recently, it has been shown that two different Ets family transcription factors, Ets1/2 and Elk1/3/4, have partially redundant activities in specifying the medial lineages of row III (a9.33 and a9.37) (Gainous et al., 2015). Our data supports these previous findings. We provide evidence that the MEK/ERK signalling pathway in row III activates *Gsx* via Ets and Elk transcription factors. We show, firstly, that the MEK/ERK signalling pathway is required for the activation of endogenous *Gsx* as well as transgene activation driven by *pGsx[-365, +11]*. We then show that dominant-negative forms of either Ets1/2 or Elk1/3/4 (EtsWRPW; ElkWRPW) are each able to repress both *Gsx* expression and transgene activation by *pGsx[-365, +11]*. We propose that both Ets/Elk factors may directly contribute to *Gsx* activation. Consistent with this idea, the -365 to +11 sequences contain several potential Ets family member binding sites (Supplementary Figure 3).

Repression mechanisms for *Gsx* expression

Gsx is repressed in column 3 by Snail transcription factor. When Snail is knocked-down, *Gsx* is ectopically expressed in column 3 at the neural plate stage (Esposito et al., 2017). Similar to endogenous *Gsx*, transgene activity driven by *pGsx[-365, +11]* is inhibited by overexpression of *Snail*. Consistent with a potential direct role, ChIP-chip analysis detected Snail binding to the upstream region of *Gsx* (Kubo et al., 2010) and potential binding sites were predicted within the -365 to +11 sequences (Supplementary Figure 3).

Previous studies have shown that *Six3/6* is specifically expressed in row IV lineages from the 6-row neural plate stage (Gainous et al., 2015; Imai et al., 2004). Restriction of *Six3/6* expression to row IV is mediated by differential ERK activation between row III and row IV cells. Inhibition of FGF/MEK/ERK signalling leads to loss of row III gene expression (including *Gsx*)

and ectopic activation of *Six3/6* in row III (Gainous et al., 2015; Haupaix et al., 2014; Racioppi et al., 2014). Six proteins can serve as transcriptional activators or repressors, depending on the presence of additional cofactors within the transcriptional complex (Li et al., 2003). Here, we show that Six3/6 is required to repress *Gsx* expression in row IV cells at the neurula stage (Figure 6C). Thus, one of the functions of Six3/6 in *Ciona* neural development involves repression of more posterior neural fates. A role for Six3/6 orthologues in repression of posterior gene expression has also been reported in other systems (Lavado et al., 2008; Leclere et al., 2016). Overexpression of Six3/6 repressed endogenous *Gsx* expression as well as transgene activity driven by *pGsx[-365, +11]*. This suggests that the *[-365, +11]* sequences contain a Six3/6 response element, an idea supported by the presence of *in silico* predicted Six-binding sites conserved between *Ciona robusta* and *Ciona savigni* (Supplementary Figure 3).

Finally, our study uncovered an element close to the transcription start site that is required to prevent both precocious and ectopic activation of *Gsx*. Both activators of *Gsx,* Delta-like (Notch) and FGF/ERK signalling are active during early gastrula stages (3-row neural plate stage), but *Gsx* is not expressed until the mid-gastrula (6-row neural plate) stage. This delay in activation could be achieved by the requirement of an additional activator, which is itself not activated until the mid-gastrula stage, or alternatively by a factor that inhibits *Gsx* transcription prior to the mid-gastrula stage. Our data lend support to the second hypothesis. Removal of the proximal sequences results in precocious and ectopic transgene activity. Differential ERK1/2 activation between dividing cells is used repeatedly during development, particularly during neural and cardiopharyngeal lineage segregations (Haupaix et al., 2014; Racioppi et al., 2014; Razy-Krajka et al., 2018; Stolfi et al., 2011; Wagner and Levine, 2012), thus late ERK targets need to be prevented from activating precociously. Indeed, this problem applies to any reiteratively used signalling pathway. One possible mechanism to correctly time gene activation would be a coherent feed forward mechanism such that a signal induces early gene targets and these targets are themselves required, together with the same activating signal, to activate the subsequent targets. This type of mechanism has been described in ascidian development during the specification of the endoderm by β-catenin signalling as well as during the specification of cardiopharyngeal mesoderm by FGF-signalling (Hudson et al., 2016; Razy-Krajka et al., 2018). Another mechanism is the presence of an inhibitory timer mechanism, which prevents the inappropriate activation of a target gene in response to an earlier activation signal. An example of this strategy was recently revealed in ascidian embryos, during the early segregation of brain from palp precursors by differential FGF signalling (Ikeda et al., 2013). In this scenario, two Blimp-like Zinc finger proteins (BZ1, BZ2) prevent the precocious FGF-dependent activation of *Zic-r.b* in palp/brain precursors prior to their lineage segregation. In the

absence of this inhibitory mechanism, brain lineage genes are expressed precociously, at the expense of palp/epidermis lineage genes and palps do not form. Furthermore, in the absence of BZ1, BZ2 and a third factor, Hes-a, *Zic-r.b* is activated even earlier in neural precursors in response to FGF, at the 32-cell stage. Thus, these factors act as a timer to delay activation of *Zic-r.b* in response to FGF signalling and this delay mechanism is critical for correct lineage segregations. We propose that a similar mechanism is taking place to prevent precocious *Gsx* activation in response to FGF at the early gastrula stage in row III/IV precursors prior to their lineage segregation. To confirm this hypothesis, it will be essential to identify the factor responsible for this time delay, repress its activity and assess if endogenous *Gsx* becomes precociously activated at earlier stages.

MATERIALS AND METHODS

Embryo experiments and tools

Adult *Ciona intestinalis* or *Ciona robus*ta were purchased from the Station Biologique de Roscoff (France) or from Stazione Zoologica Anton Dohrn (Italy), respectively. Blastomere names, lineage and the fate maps were described previously (Conklin, 1905; Nishida, 1987). Ascidian embryo culture and microinjection have been described (Sardet et al., 2011; Yasuo and McDougall, 2018). Six3/6-MO-1 (CATATCGCCGCCAGCACGTAACATA) and Six3/6-MO-3 (CCTTCACTCAACATTGATATTCTGT) were purchased from GeneTools LLC and injected into unfertilised eggs at a concentration of 0.75-1mM. In preliminary experiments with Six3/6-MO-1, ectopic expression of *Gsx* was not observed until late neurula stage (stage 15.5-16; approximately 8 hours and 20 minutes after fertilisation at 18°C). Therefore, embryos shown in Figure 6C were fixed at this stage. The electroporation protocol was based on Christiaen et al. (Christiaen et al., 2009). We used 50µg of circular plasmid DNA in 250µl of 0.6M mannitol. This solution was mixed with 100µl of eggs in artificial sea water supplemented with 0.5% BSA. Electroporation was carried out at 50V for 16ms using a BTX ECM830 (Harvard apparatus) or a BIO RAD Gene Pulser II. For co-electroporation 25µg of each plasmid DNA was used under the same conditions (in this case control single electroporations also used 25µg of DNA). All data came from at least two independent experiments (i.e. on different batches of embryos). U0126 (Calbiochem) and DAPT (Calbiochem) treatments in *Ciona* have been described previously (Hudson et al., 2003; Hudson and Yasuo, 2006).

Unique identifiers of genes analysed

Gene name	*Ciona robusta* Unique gene identity	*Ciona robusta* Unique gene model identity

Gsx	Cirobu.g00005160	KH2012:KH.C2.917
Six3/6	Cirobu.g00001582	KH2012:KH.C10.367
Snail	Cirobu.g00005955	KH2012:KH.C3.751
MEK	Cirobu.g00011301	KH2012:KH.L147.22
ETS1/2	Cirobu.g00001309	KH2012:KH.C10.113
ELK1/2/4	Cirobu.g00008865	KH2012:KH.C8.247
Notch	Cirobu.g00009697	KH2012:KH.C9.176
Delta-like	Cirobu.g00012743	KH2012:KH.L50.6

Construct preparation

The electroporation constructs *pEtr>Snail, pZic-r-b>Ets1/2, pZic-r.b>Elk1/3/4* have been previously described (Abitua et al., 2012; Gainous et al., 2015; Hudson et al., 2015). To make *pEtr>Six3/6,* the open reading frame of *Six3/6* was cloned from a cDNA clone (cicl021e08) originating from the *Ciona* gene collection plates (GC11m13) using the following primers: six3/6-F-attB1 (aaaaagcaggctaccATGGCGGAGACTGTTGCACAGCGCGCCTC) and six3/6-R-attB2 (agaaagctgggTTAGTCTTTCGGGCTCTGACTC) and subcloned into pDONR 221 P1-P2 to generate pENTR-L1-Six3/6-L2. This entry clone was mixed with pSP1.72ETR>Rfa in an LR reaction to generate *pETR>Six3/6*. Details on Gateway cloning of ascidian genes are previously published (Roure et al., 2007). To make *pSix3/6>Venus,* the *Six3/6* upstream sequences were first selected based on (Haeussler et al., 2010). The Six3/6 upstream regulatory sequences were amplified from *Ciona intestinalis* genomic DNA using the following primers: Six3/6-promoter-F : ggtcgacggtatcgataACGTCACAATGCAATGTAACGATTC and Six3/6-promoter-R2 : CATATCGCTGCCAGCACGTAACATACCTTCACTC). Venus was amplified using the following primers: Venus-F3 : GTGCTGGCAGCGATATGGTGAGCAAGGGCGAGG and Venus-R : ccgctctagaactagtgTTACTTGTACAGCTCGTCCATG. Regions of overlap between *Six3/6* and *Venus* are underlined whereas regions of overlap with the plasmid vector are in small case. Amplified DNA was gel purified and mixed with pBluescript SK linearised with HindIII and BamHI. DNA was assembled using Gibson Assembly Master Mix (New England Biolabs) according to manufacturer's protocol. *pSix3/6>Venus* was injected at a concentration of 0.03µg/µl.

For *pGsx[-3857, +11]>LacZ,* the *Ciona robusta Gsx* upstream sequences were identified by probing a cosmid library (RZPD 119 (Burgtorf et al., 1998)) with *Ciona Gsx* cDNA (Hudson and Lemaire, 2001). Sequences upstream were then sequenced from the identified cosmid (Ferrier and Holland, 2002). Approximately 4kb of sequences upstream of *Gsx* were then amplified by PCR and cloned into *psp1.72>LacZ* using the primers gsxup-3.9F and gsxR (Supplementary Table 1). Comparison of the cosmid derived sequences to the reference genome revealed 98% identity, with a 55bp insert in the cosmid sequence relative to the reference genome. This sequence corresponds to -1452 to -1398 of the *pGsx[-3857,+11]* sequences and is at position KH2012.C2.5509258 in the

reference genome. The *Gsx[-3857,+11]* cosmid derived sequences are available online (Aniseed, https://www.aniseed.cnrs.fr/aniseed/cisreg/show_cisreg?feature_id=14105022).

The 5' deleted constructs *pGsx[-1905, +11], pGsx[-829, +11], pGsx[-636, +11], pGsx[-365, +11], pGsx[-297, +11], pGsx[-256, +11], pGsx[-193, +11], pGsx[-120, +11]* were all generated by PCR using appropriate primers (see Supplementary Table 1). The 5' and 3' deleted fragments *pGsx[-297, -100], pGsx[-297, -176], pGsx[-256, -100], pGsx[-365, -236], pGsx[-256, -176], pGsx[-297, -236]* and *pGsx[-193, -100]* were all generated by PCR, using appropriate primers (Supplementary Table 2) cloned upstream of the *Brachyury* minimal promoter into *psp1.72-bpBra>LacZ* (Bertrand et al., 2003). *pGsx[-3857, -279][-120, +11]* was made by PCR (Supplementary Table 2). Constructs for the window deletion analysis described in Supplementary Figure 2 were carried out using the QuikChange Site-Directed Mutagenesis Kit (Stratagene) using the g2905D1-D8 F and R primers on *pGsx[-297, -100]bpBra* (Supplementary Table 2). All constructs were verified by sequencing.

Gsx construct name based on cosmid sequence	**Ci-Regulatory Region identifier**
pGsx[-3857, +11]	ciinte.REG.KH2012.C2.5506855- 5510677/Gsx
pGsx[-1905, +11]	ciinte.REG.KH2012.C2.5508807- 5510677/Gsx
pGsx[-829, +11]	ciinte.REG.KH2012.C2.5509831-5510677/Gsx
pGsx[-636, +11]	ciinte.REG.KH2012.C2.5510024-5510677/Gsx
pGsx[-365, +11]	ciinte.REG.KH2012.C2.5510302-5510677/Gsx
pGsx[-297, +11]	ciinte.REG.KH2012.C2.5510370- 5510677/Gsx
pGsx[-256, +11]	ciinte.REG.KH2012.C2.5510411- 5510677/Gsx
pGsx[-193, +11]	ciinte.REG.KH2012.C2.5510474- 5510677/Gsx
pGsx[-120, +11]	ciinte.REG.KH2012.C2.5510547-5510677/Gsx
pGsx[-297, -100]	ciinte.REG.KH2012.C2.5510370-5510567/Gsx
pGsx[-297, -176]	ciinte.REG.KH2012.C2.5510370-5510491/Gsx
pGsx[-256, -100]	ciinte.REG.KH2012.C2.5510411-5510567/Gsx
pGsx[-256, -176]	ciinte.REG.KH2012.C2.5510411-5510491/Gsx
pGsx[-365, -236]	ciinte.REG.KH2012.C2.5510302-5510431/Gsx
pGsx[-297, -236]	ciinte.REG.KH2012.C2.5510370-5510431/Gsx
pGsx[-193, -100]	ciinte.REG.KH2012.C2.5510474-5510567/Gsx
pGsx[-3857, -279][-120, +11]	ciinte.REG.KH2012.C2.5506855-5510388;5510547-5510677/Gsx (deleted region 5510389-5510546)

In situ hybridization and YFP immunostaining

Gsx RNA probes were synthesized from the cDNA previously reported (Hudson and Lemaire 2001). Whole-mount in situ hybridizations were performed as previously described (Hudson and Yasuo, 2006; Ristoratore et al., 1999; Wada et al., 1995). For nuclear staining, embryos were mounted in Vectashield-DAPI (Vector laboratories). Bright-field and DAPI images were merged with Adobe Photoshop. YFP immunostaining (Supplementary Figure 4) was carried out using a

Goat-anti-GFP (Rockland immunochemicals 600-101-215; 1/250) followed by Donkey anti-goat Alexaflour 555 (A-21432 Thermofischer; 1/250). Confocal analysis of immunostained larvae was performed with a Leica SP5 or SP8 microscope and image stacks were produced with Fiji (ImageJ 2.0.0) software (Schindelin et al., 2012).

Statistical tests

For statistical tests, contingency tables were made with the total numbers of embryos pooled from all experiments for each outcome (positive, negative, weak, ectopic). Fischer's exact tests or Chi-square tests were carried out using Prism version 8.0.0 (for MacOS, GraphPad Software, La Jolla California USA, www.graphpad.com). All contingency tables can be found in Supplementary information (Supplementary Table 3).

In Silico transcription factor binding site searches

The -365 to +11 regulatory sequence was searched for transcription factor binding sites for 3 transcription factors using *Ciona robusta* SELEX-seq data (best cycle as indicated in ANISEED)(Brozovic et al., 2018). For each 8-mer in the *Ciona robusta* and *Ciona savignyi* genomes, we first calculated a raw local affinity for a given transcription factor as the sum of the log enrichment scores of the three 6-mers included in each 8-mer. These raw values were normalized to decrease their dependency on the global enrichment achieved during SELEX-seq, thereby facilitating comparison between factors within and across families. For each transcription factor, we plotted the histogram of raw affinity scores for each possible 8-mer (65536) and assigned a normalized score of 0 to the 8-mers with a raw score corresponding to the peak of the histogram. The -1 value was assigned to the 0.1% worst 8-mers, while the maximal +1 value was assigned to the 0.1% best 8-mers. Values between -1 and 0 and 0 and +1 were scaled linearly. This normalized affinity score is allocated to the fourth base of each 8-mer. To focus on the most likely binding sites, we identified the summit of each peak, to which the histogram value for this base was allocated. We further filtered this dataset to keep only the top 10% of highest peaks.

We expect functional peaks to be conserved across closely related species. To identify conserved peaks, we used the ANISEED genome alignments of *Ciona robusta* and *Ciona savignyi* obtained by running LastZ (v1.02.00) on masked genomes (http://www.bx.psu.edu/~rsharris/lastz/ ; (Harris, 2007)), with the following parameters (hsp_threshold = 3000; gapped_threshold = 3000; x_drop = 870; y_drop = 6290; gap_open_penalty = 290; gap_extend_penalty = 20) and the following score matrix, computed to improve the alignment between the two species.

```
#      A      C      G      T
#  A  87  -119   -55  -112
#  C -119  100  -154  -55
#  G  -55  -154   100  -119
#  T -112  -55   -119   87
```

Matching *Ciona robusta* and *Ciona savignyi* peaks, distant by at most 5 bp in the alignment between the two species, were considered conserved and allocated the product of the peak values in each species.

Acknowlegements:

We would like to thank Philip Abitua (UC Berkeley, now Harvard University), Ignacio Navarrete (UC Berkeley) and Mike Levine (UCLA, now Princeton University) for kindly sharing the Ets and Elk activator and repressor constructs and Nori Satoh and colleagues for the *Ciona* gene collection plates. Many thanks to Christelle Dantec (CRBM, CNRS) for helping with SELEX-seq data processing and *Ciona* genome alignments. The team of H. Y. are supported by the Centre National de la Recherche Scientifique (CNRS), the Université Pierre et Marie Curie, and the Agence Nationale de la Recherche (ANR-09-BLAN-0013-01 ; ANR-17-CE13-0003-01). Work by R. E. in the laboratory of H. Y. was supported by an EMBO short term fellowship (ASTF 534-2014). Work by P. L. and E. F. was supported by CNRS and the Agence Nationale de la Recherche (ANR-13-BSV2-0011-01,TED ; ANR-08-BLAN-0067, Chor-Evo-Net). Work by R. E., A. P. and L. S. in the laboratory of A. S. was supported by SZN PhD fellowships. The group of D. E. K. F. is supported by the Leverhulme Trust (RPG-2016-351). Isolation of the *Gsx* containing cosmid was conducted in the laboratory of Peter Holland and supported by the BBSRC (no. G09218).

FIGURE LEGENDS

Figure 1

Comparison of endogenous *Gsx* expression with transgene expression driven by the upstream regulatory sequences of *Gsx*. Stage of analysis is shown on the left. The left column shows endogenous *Gsx* expression. The middle and right columns are embryos electroporated with *pGsx[-3857, +11]>LacZ.* The middle column shows expression of the *LacZ* reporter gene detected by in situ hybridisation against *LacZ.* The right-hand column shows β- galactosidase detection. Note the time lag between *LacZ* and β-galactosidase detection. A schematic drawing of neural plate cells is shown on the right for neural plate and neurula stage embryos, with the *Gsx* positive cells labelled in red.

Figure 2

5' deletion analysis of the [-3857, +11] regulatory sequences of *Gsx.* Top is a schematic representation of the [-3857, +11] *Gsx* regulatory sequences. The graph summarises multiple experiments. Shown are the mean and standard deviation of percentages of neurula stage embryos positive for β-galactosidase activity in the neural cells. Each construct was electroporated in parallel with the control *pGsx[-3857, +11]* construct. Above each histogram bar is the total number of embryos analysed, with the number of independent experiments indicated in the brackets. Statistical tests compared each deletion construct (blue bars) to the corresponding control ([-3857, +11] red bars). For the statistical tests, contingency tables were made with the proportions of embryos positive or negative (Supplementary table 3) and analysed by Fischer's exact test. ns= non-significant; ****= P<0.0001. Below the graph are representative embryos for some constructs. The blue cells in the embryos electroporated with *pGsx[-193, +11]* and *pGsx[-120, +11]* are non-neural cells.

Figure 3

Window deletion analysis around the [-256, -193] sequences. A) Fragments of *Gsx* upstream sequences cloned are indicated with unbroken lines. The black rectangle represents the minimal *Brachyury* promoter (*bpBra*). Ticks indicate active constructs and crosses inactive constructs. B) The construct content (in *pGsx[n, n]bpBra*) is shown below the bars of the three histograms. The graphs summarize multiple experiments. Top: shown are the mean and standard deviation of percentages of neurula stage embryos positive for β-galactosidase activity in the neural cells for each construct compared to the corresponding control ([-3857, +11] red bars) electroporations conducted in parallel. Comparing the proportion of embryos positive or negative relative to the

corresponding control (full construct [-3857, +11]) indicates that each construct is significantly different (P<0.0001) compared to the full construct (Fischer's exact test). Above each histogram bar is the total number of embryos analysed, with the number of independent experiments indicated in the brackets. Middle (green box): the graph shows the mean and standard deviations of the percentage of embryos positive for neural β-galactosidase activity (from the top graph) that exhibited ectopic lateral β-galactosidase activity. Bottom (blue box); the graph shows the mean and standard deviations of the percentage of embryos positive for neural β-galactosidase activity that exhibited ectopic anterior β-galactosidase activity. On the middle graph is indicated the total number of neural-positive embryos analysed for lateral or anterior expansion of β-galactosidase activity. Middle and Bottom graphs: differences in the levels of ectopic expression between certain deletion constructs and the corresponding controls (full construct [-3857, +11]) was supported by statistical analysis. For the statistical tests, contingency tables were made with the proportions of positive embryos exhibiting ectopic or no ectopic activity (Supplementary table 3) and analysed by Fischer's exact test. ns= non-significant; ****= P<0.0001. Statistical tests for [-256, -175], [-297, -236] and [-193, -100] were not conducted due to low numbers of positive embryos. C) Representative embryos showing normal β-galactosidase (left), anterior and lateral expansion (middle) and lateral expansion (right). Schematics indicate normal (red) and ectopic (blue for anterior and green for lateral) expression. Asterisks indicate 'mesenchyme' ectopic activity.

Figure 4

Role of MEK and Ets family members in *Gsx* gene regulation. Graphs show the mean and standard deviation of percentages of neurula stage embryos positive for β-galactosidase activity in the neural cells or for *Gsx* gene expression, under the conditions indicated. Above each histogram bar is the total number of embryos analysed, with the number of independent experiments indicated in the brackets. A) *Gsx* expression following U0126 treatment. B) Neural β-galactosidase activity in embryos electroporated with *pGsx[-365, +11]* and treated with U0126. C) *Gsx* expression in embryos electroporated with *pZic-r.b>EtsVP16* or *pZic-r.b>EtsWRPW*. Each half embryo was scored independently. D) Neural β-galactosidase activity in embryos electoporated with *pGsx[-365, +11]* or co-electroporated with *pGsx[-365, +11]* and *pZic-r.b>EtsVP16* or *pZic-r.b>EtsWRPW*. E) Neural β-galactosidase activity in embryos electoporated with *pGsx[-365, +11]* or co-electroporated with *pGsx[-365, +11]* and *pZic-r.b>ElkVP64* or *pZic-r.b>ElkWRPW*. F) *Gsx* expression in embryos electroporated with *pZic-r.b>ElkVP64* or *pZic-r.b>ElkWRPW*. Statistical tests compared each experimental condition (blue bars) to the corresponding controls (red bars). For the statistical tests, contingency tables were made with the proportions of embryos positive,

negative or weak (Supplementary table 3) and analysed by Fischer's exact test (A, B, D, E) or Chi square (C, F). ns= non-significant; ****= P<0.0001. In C) *pZic-r.b>EtsVP16* embryos were also compared to *pZic-r.b>EtsWRPW* embryos (Fischer's exact test, P<0.0001).

Figure 5

The *pGsx[-365, +11]* sequences contain a Snail and Notch response element. Graphs show the mean and standard deviation of percentages of neurula stage embryos positive for β-galactosidase activity in the neural cells under the conditions indicated. Above each histogram bar is the total number of embryos analysed, with the number of independent experiments indicated in the brackets. A) Embryos electoporated with *pGsx[-365, +11]* and treated with DAPT. B) Embryos electoporated with *pGsx[-365, +11]* or co-electroporated with *pGsx[-365, +11]* and *pEtr>Snail*. Statistical tests compared each experimental condition (blue bars) to the corresponding controls (red bars). For the statistical tests, contingency tables were made with the proportions of embryos positive or negative (Supplementary table 3) and analysed by Fischer's exact test. ****= P<0.0001.

Figure 6

Role of Six3/6 in *Gsx* gene regulation. A, B, D) Graphs show the mean and standard deviation of percentages of neurula stage embryos positive for β-galactosidase activity in the neural cells or for *Gsx* gene expression, under the conditions indicated. Above each histogram bar is the total number of embryos analysed, with the number of independent experiments indicated in the brackets. A) *Gsx* expression in embryos electroporated with *pEtr>LacZ* or *pEtr>Six3/6*. Each half embryo was scored independently. B) Neural β-galactosidase activity in embryos electoporated with *pGsx[-365, +11]* or co-electroporated with *pGsx[-365, +11]* and *pEtr>Six3/6*. C) Expression of *Gsx* in Six3/6-MO-1 or Six3/6-MO-3 injected embryos. At late neurula stages, ectopic *Gsx* is visible in anterior cells (row IV) of Six3/6-MO injected embryos (red arrows). Numbers indicate total number of embryos analysed with numbers in brackets indicating the number of independent experiments. The graph shows the proportion of embryos with ectopic row IV *Gsx* gene expression. D) Neural β-galactosidase activity in embryos electoporated with the *pGsx* constructs and *pEtr>Six3/6* as indicated below. On the right are representative embryos. Statistical tests compared each experimental condition to the corresponding controls. For the statistical tests, contingency tables were made with the proportions of embryos (where appropriate-positive, negative, weak, ectopic) (Supplementary table 3) and analysed by Fischer's exact test (B, C) or Chi square (A, D). ****= P<0.0001.

Figure 7

The [-235, +11] sequences contain a temporal regulatory element. Top: Graph shows the mean and standard deviation of percentages of embryos with β-galactosidase activity in the neural cells in embryos electoporated with *pGsx[-365, +11]* or *pGsx[-365, -236]bpBra* at the 6-row neural plate stage, 30 minutes later (+30 minutes) or 60 minutes later (+60 minutes). Above each histogram bar is the total number of embryos analysed, with the number of independent experiments indicated in the brackets. Below are representative embryos at +30 minutes and +60 minutes time points. Rows III and IV and columns 2 and 3 are labelled to show staining patterns. Below each representative embryo panel are the respective percentages of positive embryos that displayed ectopic anterior (row IV) or lateral (column 3) β-galactosidase activity. Statistical tests compared each experimental condition to the corresponding controls. For the statistical tests, contingency tables were made with the proportions of embryos positive or negative (Supplementary table 3) and analysed by Fischer's exact test. ns= non-significant; ****= $P<0.0001$.

Figure 8

A schematic representation of the cis-regulatory region of *Ciona Gsx*, summarizing our main conclusions.

Supplementary Figures

Supplementary Figure 1

Deletion of the -278 to -121 sequences from the *pGsx[-3857, +11]* construct. Top is a schematic representation of the constructs analysed. The graph shows the mean and standard deviation of percentages of neurula stage embryos positive for β-galactosidase activity in the neural cells. Above each histogram bar is the total number of embryos analysed, with the number of independent experiments indicated in the brackets. The basal promoter was not removed from this construct since the *Gsx[-120, +11]* sequences are able to drive expression of an *Otx* enhancer (Bertrand et al, 2003).

Supplementary Figure 2

A serial window deletion across the -256 to -100 region in *pGsx[-297, -100]bpbra>LacZ.* A) Deleted regions are indicated as Dn (example D1, D2 etc). Positions used in previous deletion analysis are indicated.The green bar indicates a perfect match to the Su(H) consensus binding site. B) The graph shows the mean and standard deviation of percentages of neurula stage embryos positive for β-galactosidase activity in the neural cells. Above each histogram bar is the total number of embryos analysed, with the number of independent experiments indicated in the brackets. Statistical tests compared each experimental condition (blue bars) to the corresponding control (red bar). For the statistical tests, contingency tables were made with the proportions of embryos positive or negative (Supplementary table 3) and analysed by Fischer's exact test. ns= non-significant; *= P<0.05; ** =P< 0.01; ***= P<0.001; ****= P<0.0001.

Supplementary Figure 3

In silico predicted binding profiles for 3 different transcription factors, Six3/6, Snail and Ets on the region from 5510 to 5511 of chromosome 2, based on SELEX-seq data. The -365 to +11 sequences are depicted by the blue box. The first group of tracks (GSX-CI-CS-NORMALIZE_CI-8SELEX) attributes to each base a score reflecting the predicted affinity of the TFs to the target DNA, based on SELEX-seq 6-mer enrichment counts (see methods). The second group of tracks (GSX-CI-CS-PEAKS_NORMALIZE_CI-8SELEX) only represents the local maxima (subsequently called peaks) of the previous group of tracks. The third group of tracks (GSX-CI-CS-10PER_PEAKS_NORMALIZE_CI-8SELEX) shows only the top 10% highest peaks. In the fourth group of tracks (GSCI-CS-5CONS_10PER), are only kept the peaks conserved between the two species (see methods) to which we associated a score value obtained by multiplying the peak

heights in both species. The tracks KH2012 transcript model show the position of the *Gsx* gene. The bottom track shows the local score of sequence conservation between *Cirobu* and *Cisavi*.

Supplementary Figure 4

The Six3/6-MOs recognise their target sites. A) Construct used in assay designed to test whether the Six3/6-MOs act as sequence specific translational blockers. 2.1kb of the upstream regulatory sequences of Six3/6 (blue), containing the two non-overlapping MO target sites, were fused (red) with Venus YFP (green). This construct, *pSix3/6>Venus*, was injected into embryos with or without a Six3/6-MO and assayed for YFP protein in the anterior nervous system (B). B) On the left are confocal stacks of control (*pSix3/6>Venus*) and MO-injected (*pSix3/6>Venus* +MO) larva. The proportion of embryos scored for positive, weak (barely detectable) or negative detection of YFP protein are indicated on the graph. Fischer's exact tests compared MO injected embryos to controls. ****= P<0.0001.

Supplementary Table 1

Primer sequences used to generate the deletion series presented in Figure 2.

Supplementary Table 2

Primer sequences used to generate the window deletion series presented in Figure 3 and Supplementary Figure 2.

Supplementary Table 3

Contingency tables used for the Fisher's exact and Chi square statistical tests.

REFERENCES

Abitua, P.B., Wagner, E., Navarrete, I.A., Levine, M., 2012. Identification of a rudimentary neural crest in a non-vertebrate chordate. Nature 492, 104-107.

Bertrand, V., Hudson, C., Caillol, D., Popovici, C., Lemaire, P., 2003. Neural tissue in ascidian embryos is induced by FGF9/16/20, acting via a combination of maternal GATA and Ets transcription factors. Cell 115, 615-627.

Brozovic, M., Dantec, C., Dardaillon, J., Dauga, D., Faure, E., Gineste, M., Louis, A., Naville, M., Nitta, K.R., Piette, J., Reeves, W., Scornavacca, C., Simion, P., Vincentelli, R., Bellec, M., Aicha, S.B., Fagotto, M., Gueroult-Bellone, M., Haeussler, M., Jacox, E., Lowe, E.K., Mendez, M., Roberge, A., Stolfi, A., Yokomori, R., Brown, C.T., Cambillau, C., Christiaen, L., Delsuc, F., Douzery, E., Dumollard, R., Kusakabe, T., Nakai, K., Nishida, H., Satou, Y., Swalla, B., Veeman, M., Volff, J.N., Lemaire, P., 2018. ANISEED 2017: extending the integrated ascidian database to the exploration and evolutionary comparison of genome-scale datasets. Nucleic Acids Res 46, D718-D725.

Burgtorf, C., Welzel, K., Hasenbank, R., Zehetner, G., Weis, S., Lehrach, H., 1998. Gridded genomic libraries of different chordate species: a reference library system for basic and comparative genetic studies of chordate genomes. Genomics 52, 230-232.

Christiaen, L., Wagner, E., Shi, W., Levine, M., 2009. Electroporation of transgenic DNAs in the sea squirt Ciona. Cold Spring Harb Protoc 2009, pdb prot5345.

Cole, A.G., Meinertzhagen, I.A., 2004. The central nervous system of the ascidian larva: mitotic history of cells forming the neural tube in late embryonic Ciona intestinalis. Dev Biol 271, 239-262.

Conklin, E.G., 1905. The organisation and cell lineage of the ascidian egg. J..Acad. Nat. Sci. Philadelphia 13, 1-119.

Davidson, B., Shi, W., Beh, J., Christiaen, L., Levine, M., 2006. FGF signaling delineates the cardiac progenitor field in the simple chordate, Ciona intestinalis. Genes Dev 20, 2728-2738.

Esposito, R., Yasuo, H., Sirour, C., Palladino, A., Spagnuolo, A., Hudson, C., 2017. Patterning of brain precursors in ascidian embryos. Development 144, 258-264.

Ferrier, D.E., Holland, P.W., 2002. Ciona intestinalis ParaHox genes: evolution of Hox/ParaHox cluster integrity, developmental mode, and temporal colinearity. Mol Phylogenet Evol 24, 412-417.

Fortini, M.E., Artavanis-Tsakonas, S., 1994. The suppressor of hairless protein participates in notch receptor signaling. Cell 79, 273-282.

Gainous, T.B., Wagner, E., Levine, M., 2015. Diverse ETS transcription factors mediate FGF signaling in the Ciona anterior neural plate. Dev Biol 399, 218-225.

Haeussler, M., Jaszczyszyn, Y., Christiaen, L., Joly, J.S., 2010. A cis-regulatory signature for chordate anterior neuroectodermal genes. PLoS Genet 6, e1000912.

Harris, R.S., 2007. Improved pairwise alignment of genomic DNA. Ph.D. Thesis, The Pennsylvania State University.

Haupaix, N., Abitua, P.B., Sirour, C., Yasuo, H., Levine, M., Hudson, C., 2014. Ephrin-mediated restriction of ERK1/2 activity delimits the number of pigment cells in the Ciona CNS. Dev Biol 394, 170-180.

Hotta, K., Mitsuhara, K., Takahashi, H., Inaba, K., Oka, K., Gojobori, T., Ikeo, K., 2007. A web-based interactive developmental table for the ascidian Ciona intestinalis, including 3D real-image embryo reconstructions: I. From fertilized egg to hatching larva. Dev Dyn 236, 1790-1805.

Hudson, C., 2016. The central nervous system of ascidian larvae. Wiley Interdiscip Rev Dev Biol 5, 538-561.

Hudson, C., Darras, S., Caillol, D., Yasuo, H., Lemaire, P., 2003. A conserved role for the MEK signalling pathway in neural tissue specification and posteriorisation in the invertebrate chordate, the ascidian Ciona intestinalis. Development 130, 147-159.
Hudson, C., Lemaire, P., 2001. Induction of anterior neural fates in the ascidian Ciona intestinalis. Mech Dev 100, 189-203.
Hudson, C., Lotito, S., Yasuo, H., 2007. Sequential and combinatorial inputs from Nodal, Delta2/Notch and FGF/MEK/ERK signalling pathways establish a grid-like organisation of distinct cell identities in the ascidian neural plate. Development 134, 3527-3537.
Hudson, C., Sirour, C., Yasuo, H., 2015. Snail mediates medial-lateral patterning of the ascidian neural plate. Dev Biol 403, 172-179.
Hudson, C., Sirour, C., Yasuo, H., 2016. Co-expression of Foxa.a, Foxd and Fgf9/16/20 defines a transient mesendoderm regulatory state in ascidian embryos. Elife 5.
Hudson, C., Yasuo, H., 2005. Patterning across the ascidian neural plate by lateral Nodal signalling sources. Development 132, 1199-1210.
Hudson, C., Yasuo, H., 2006. A signalling relay involving Nodal and Delta ligands acts during secondary notochord induction in Ciona embryos. Development 133, 2855-2864.
Ikeda, T., Matsuoka, T., Satou, Y., 2013. A time delay gene circuit is required for palp formation in the ascidian embryo. Development 140, 4703-4708.
Imai, K.S., Hino, K., Yagi, K., Satoh, N., Satou, Y., 2004. Gene expression profiles of transcription factors and signaling molecules in the ascidian embryo: towards a comprehensive understanding of gene networks. Development 131, 4047-4058.
Imai, K.S., Levine, M., Satoh, N., Satou, Y., 2006. Regulatory blueprint for a chordate embryo. Science 312, 1183-1187.
Kubo, A., Suzuki, N., Yuan, X., Nakai, K., Satoh, N., Imai, K.S., Satou, Y., 2010. Genomic cis-regulatory networks in the early Ciona intestinalis embryo. Development 137, 1613-1623.
Kumar, J.P., 2009. The sine oculis homeobox (SIX) family of transcription factors as regulators of development and disease. Cell Mol Life Sci 66, 565-583.
Lavado, A., Lagutin, O.V., Oliver, G., 2008. Six3 inactivation causes progressive caudalization and aberrant patterning of the mammalian diencephalon. Development 135, 441-450.
Leclere, L., Bause, M., Sinigaglia, C., Steger, J., Rentzsch, F., 2016. Development of the aboral domain in Nematostella requires beta-catenin and the opposing activities of Six3/6 and Frizzled5/8. Development 143, 1766-1777.
Li, X., Oghi, K.A., Zhang, J., Krones, A., Bush, K.T., Glass, C.K., Nigam, S.K., Aggarwal, A.K., Maas, R., Rose, D.W., Rosenfeld, M.G., 2003. Eya protein phosphatase activity regulates Six1-Dach-Eya transcriptional effects in mammalian organogenesis. Nature 426, 247-254.
Meinertzhagen, I.A., Lemaire, P., Okamura, Y., 2004. The neurobiology of the ascidian tadpole larva: recent developments in an ancient chordate. Annu Rev Neurosci 27, 453-485.
Mita, K., Fujiwara, S., 2007. Nodal regulates neural tube formation in the Ciona intestinalis embryo. Dev Genes Evol 217, 593-601.
Navarrete, I.A., Levine, M., 2016. Nodal and FGF coordinate ascidian neural tube morphogenesis. Development 143, 4665-4675.
Nicol, D., Meinertzhagen, I.A., 1988. Development of the central nervous system of the larva of the ascidian, Ciona intestinalis L. I. The early lineages of the neural plate. Dev Biol 130, 721-736.
Nieto, M.A., 2002. The snail superfamily of zinc-finger transcription factors. Nat Rev Mol Cell Biol 3, 155-166.
Nishida, H., 1987. Cell lineage analysis in ascidian embryos by intracellular injection of a tracer enzyme. III. Up to the tissue restricted stage. Dev Biol 121, 526-541.
Nishida, H., 2003. Spatio□temporal pattern of MAP kinase activation in embryos of the ascidian Halocynthia roretzi. development, Growth & Differentiation 45, 27-37.

Oda-Ishii, I., Bertrand, V., Matsuo, I., Lemaire, P., Saiga, H., 2005. Making very similar embryos with divergent genomes: conservation of regulatory mechanisms of Otx between the ascidians Halocynthia roretzi and Ciona intestinalis. Development 132, 1663-1674.
Racioppi, C., Kamal, A.K., Razy-Krajka, F., Gambardella, G., Zanetti, L., di Bernardo, D., Sanges, R., Christiaen, L.A., Ristoratore, F., 2014. Fibroblast growth factor signalling controls nervous system patterning and pigment cell formation in Ciona intestinalis. Nat Commun 5, 4830.
Razy-Krajka, F., Gravez, B., Kaplan, N., Racioppi, C., Wang, W., Christiaen, L., 2018. An FGF-driven feed-forward circuit patterns the cardiopharyngeal mesoderm in space and time. Elife 7.
Ristoratore, F., Spagnuolo, A., Aniello, F., Branno, M., Fabbrini, F., Di Lauro, R., 1999. Expression and functional analysis of Cititf1, an ascidian NK-2 class gene, suggest its role in endoderm development. Development 126, 5149-5159.
Roure, A., Rothbacher, U., Robin, F., Kalmar, E., Ferone, G., Lamy, C., Missero, C., Mueller, F., Lemaire, P., 2007. A multicassette Gateway vector set for high throughput and comparative analyses in ciona and vertebrate embryos. PLoS One 2, e916.
Sardet, C., McDougall, A., Yasuo, H., Chenevert, J., Pruliere, G., Dumollard, R., Hudson, C., Hebras, C., Le Nguyen, N., Paix, A., 2011. Embryological methods in ascidians: the Villefranche-sur-Mer protocols. Methods Mol Biol 770, 365-400.
Satou, Y., Mineta, K., Ogasawara, M., Sasakura, Y., Shoguchi, E., Ueno, K., Yamada, L., Matsumoto, J., Wasserscheid, J., Dewar, K., Wiley, G.B., Macmil, S.L., Roe, B.A., Zeller, R.W., Hastings, K.E., Lemaire, P., Lindquist, E., Endo, T., Hotta, K., Inaba, K., 2008. Improved genome assembly and evidence-based global gene model set for the chordate Ciona intestinalis: new insight into intron and operon populations. Genome Biol 9, R152.
Schindelin, J., Arganda-Carreras, I., Frise, E., Kaynig, V., Longair, M., Pietzsch, T., Preibisch, S., Rueden, C., Saalfeld, S., Schmid, B., Tinevez, J.Y., White, D.J., Hartenstein, V., Eliceiri, K., Tomancak, P., Cardona, A., 2012. Fiji: an open-source platform for biological-image analysis. Nat Methods 9, 676-682.
Squarzoni, P., Parveen, F., Zanetti, L., Ristoratore, F., Spagnuolo, A., 2011. FGF/MAPK/Ets signaling renders pigment cell precursors competent to respond to Wnt signal by directly controlling Ci-Tcf transcription. Development 138, 1421-1432.
Stolfi, A., Wagner, E., Taliaferro, J.M., Chou, S., Levine, M., 2011. Neural tube patterning by Ephrin, FGF and Notch signaling relays. Development 138, 5429-5439.
Taniguchi, K., Nishida, H., 2004. Tracing cell fate in brain formation during embryogenesis of the ascidian Halocynthia roretzi. Development, growth & differentiation 46, 163-180.
Veeman, M.T., Newman-Smith, E., El-Nachef, D., Smith, W.C., 2010. The ascidian mouth opening is derived from the anterior neuropore: reassessing the mouth/neural tube relationship in chordate evolution. Dev Biol 344, 138-149.
Wada, S., Katsuyama, Y., Yasugi, S., Saiga, H., 1995. Spatially and temporally regulated expression of the LIM class homeobox gene Hrlim suggests multiple distinct functions in development of the ascidian, Halocynthia roretzi. Mech Dev 51, 115-126.
Wada, S., Tokuoka, M., Shoguchi, E., Kobayashi, K., Di Gregorio, A., Spagnuolo, A., Branno, M., Kohara, Y., Rokhsar, D., Levine, M., Saiga, H., Satoh, N., Satou, Y., 2003. A genomewide survey of developmentally relevant genes in Ciona intestinalis. II. Genes for homeobox transcription factors. Dev Genes Evol 213, 222-234.
Wagner, E., Levine, M., 2012. FGF signaling establishes the anterior border of the Ciona neural tube. Development 139, 2351-2359.
Yasuo, H., Hudson, C., 2007. FGF8/17/18 functions together with FGF9/16/20 during formation of the notochord in Ciona embryos. Dev Biol 302, 92-103.
Yasuo, H., McDougall, A., 2018. Practical Guide for Ascidian Microinjection: Phallusia mammillata. Adv Exp Med Biol 1029, 15-24.

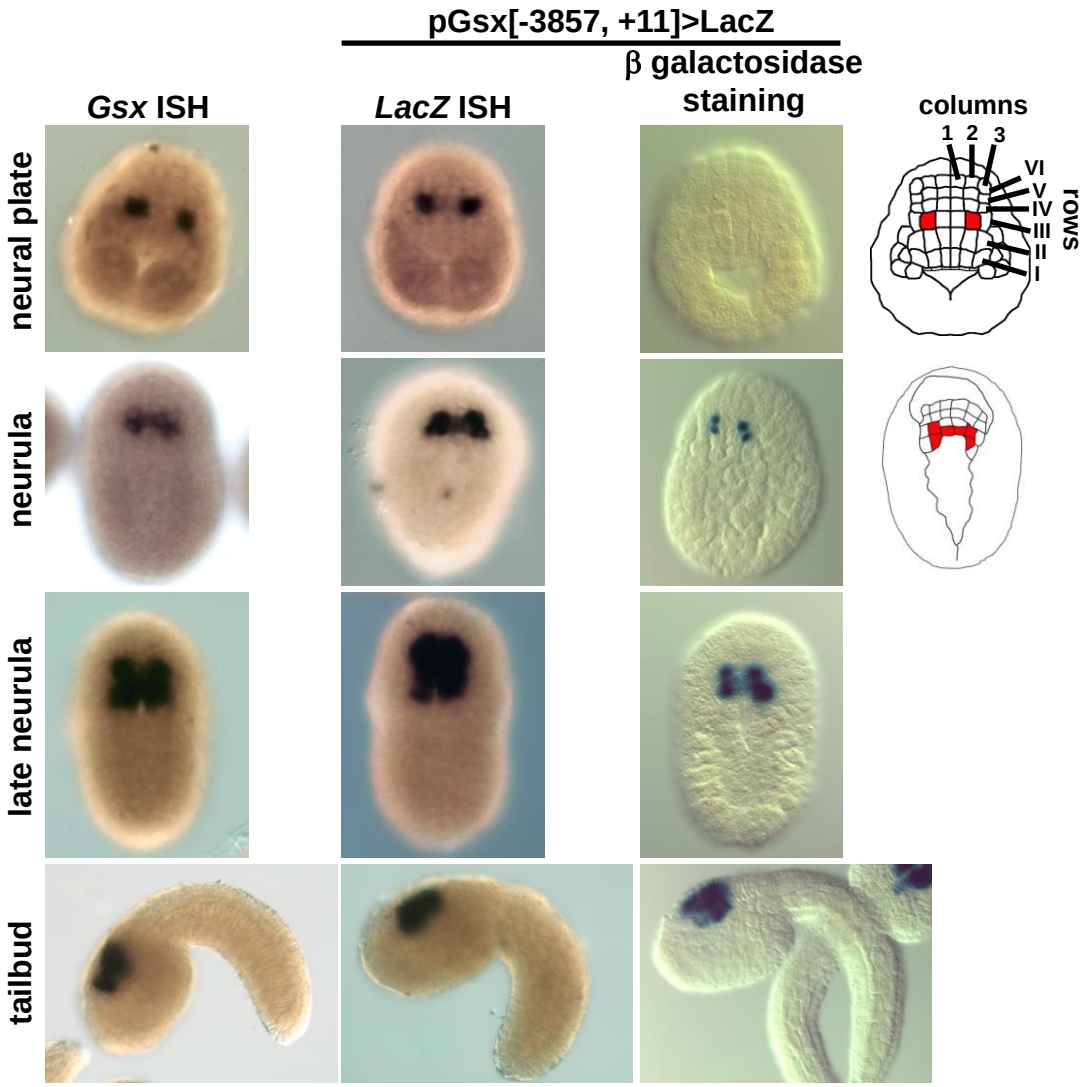
pGsx[-3857, +11]>LacZ
β galactosidase staining
Gsx ISH
LacZ ISH
columns
1 2 3
VI
V
IV
III
II
I
rows
neural plate
neurula
late neurula
tailbud

Figure 1

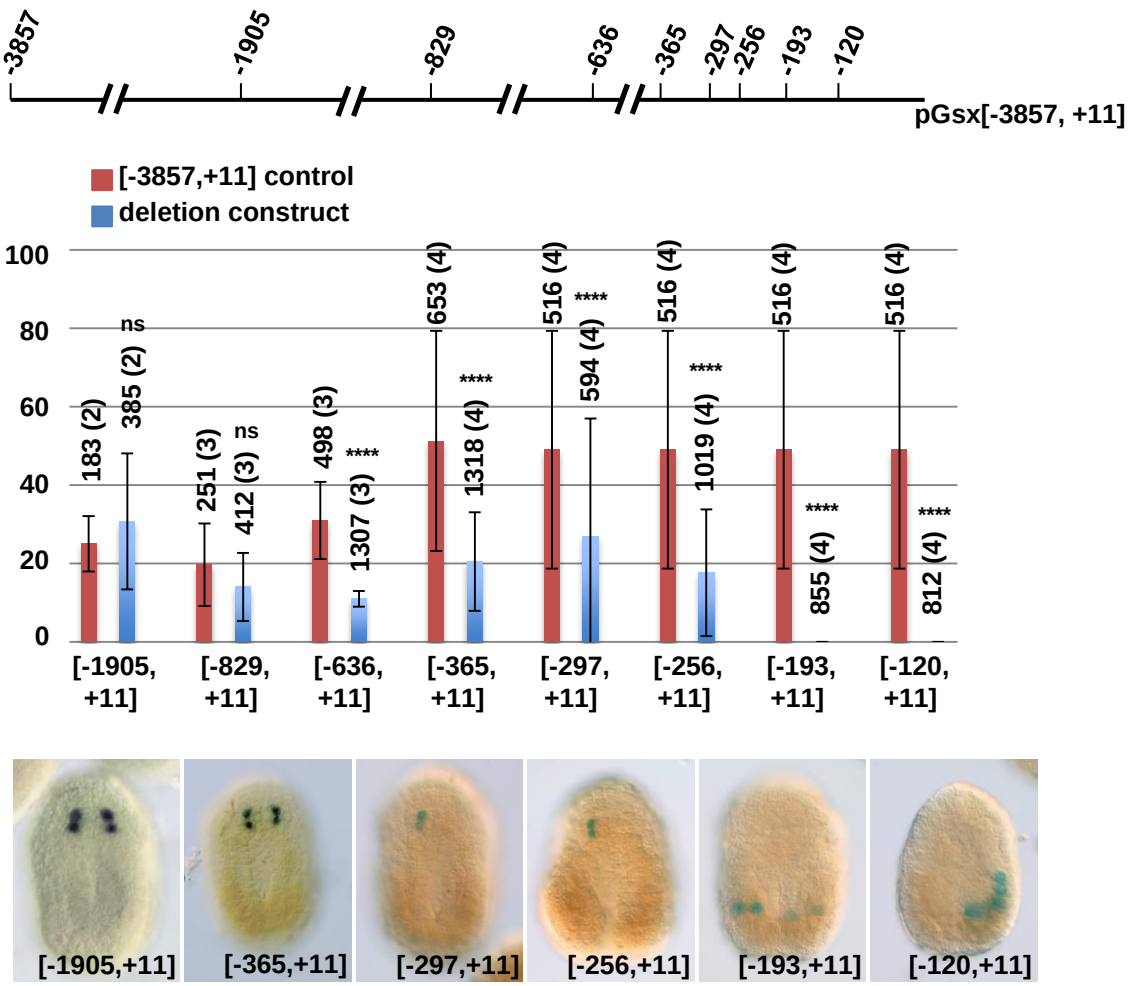
-3857
-1905
-829
-636
-365
-297
-256
-193
-120
pGsx[-3857, +11]
[-3857,+11] control
deletion construct
100
80
60
40
20
0
183 (2)
385 (2)
ns
251 (3)
412 (3)
ns
498 (3)
1307 (3)
****
653 (4)
1318 (4)
****
516 (4)
594 (4)
****
516 (4)
1019 (4)
****
516 (4)
855 (4)
****
516 (4)
812 (4)
****
[-1905, +11]
[-829, +11]
[-636, +11]
[-365, +11]
[-297, +11]
[-256, +11]
[-193, +11]
[-120, +11]
[-1905,+11]
[-365,+11]
[-297,+11]
[-256,+11]
[-193,+11]
[-120,+11]

Figure 2

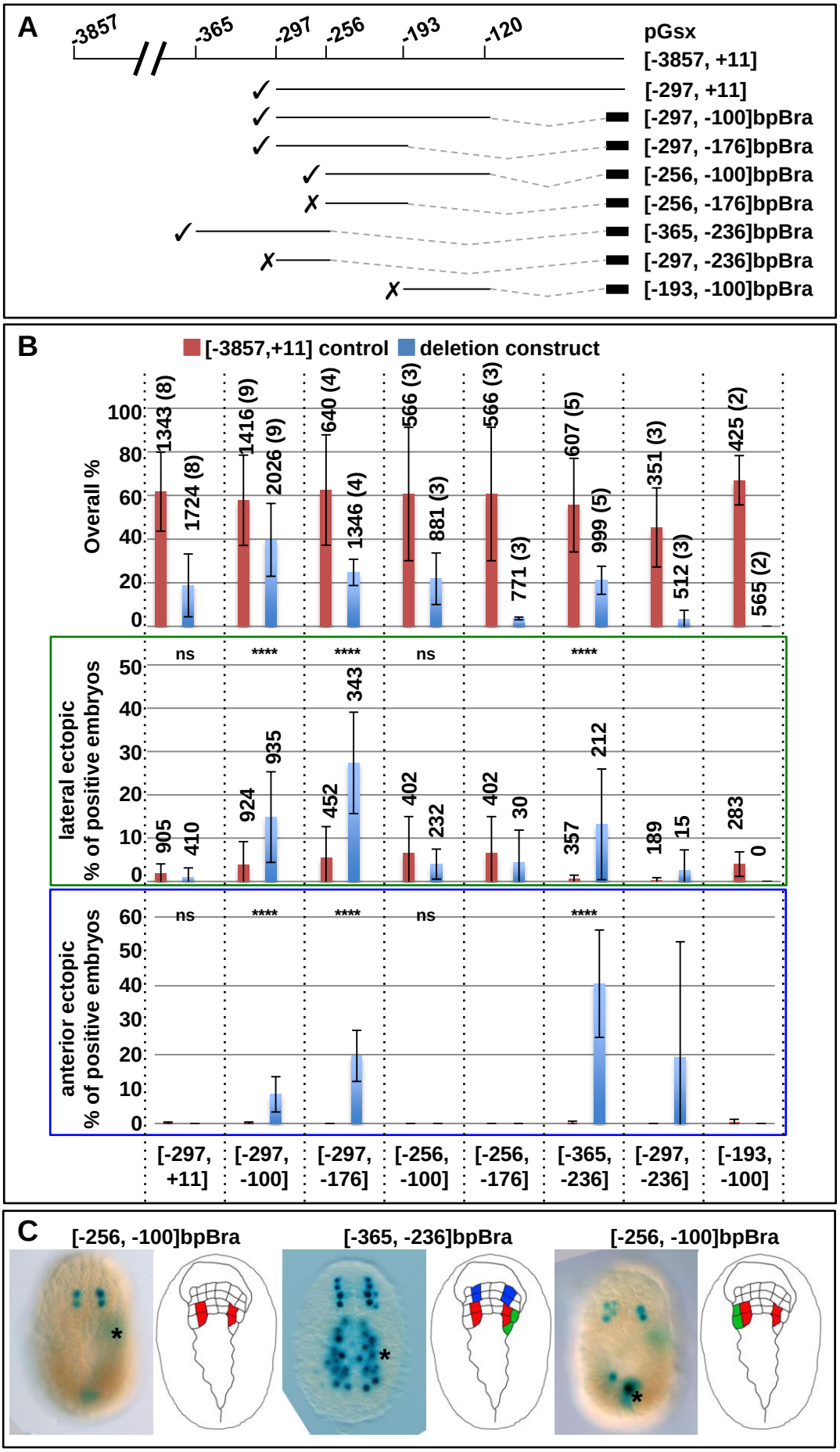
A
-3857
-365
-297
-256
-193
-120
pGsx
[-3857, +11]
[-297, +11]
[-297, -100]bpBra
[-297, -176]bpBra
[-256, -100]bpBra
[-256, -176]bpBra
[-365, -236]bpBra
[-297, -236]bpBra
[-193, -100]bpBra
B
[-3857,+11] control
deletion construct
Overall %
lateral ectopic % of positive embryos
anterior ectopic % of positive embryos
ns
****
[-297, +11]
[-297, -100]
[-297, -176]
[-256, -100]
[-256, -176]
[-365, -236]
[-297, -236]
[-193, -100]
C
[-256, -100]bpBra
[-365, -236]bpBra
[-256, -100]bpBra

Figure 3

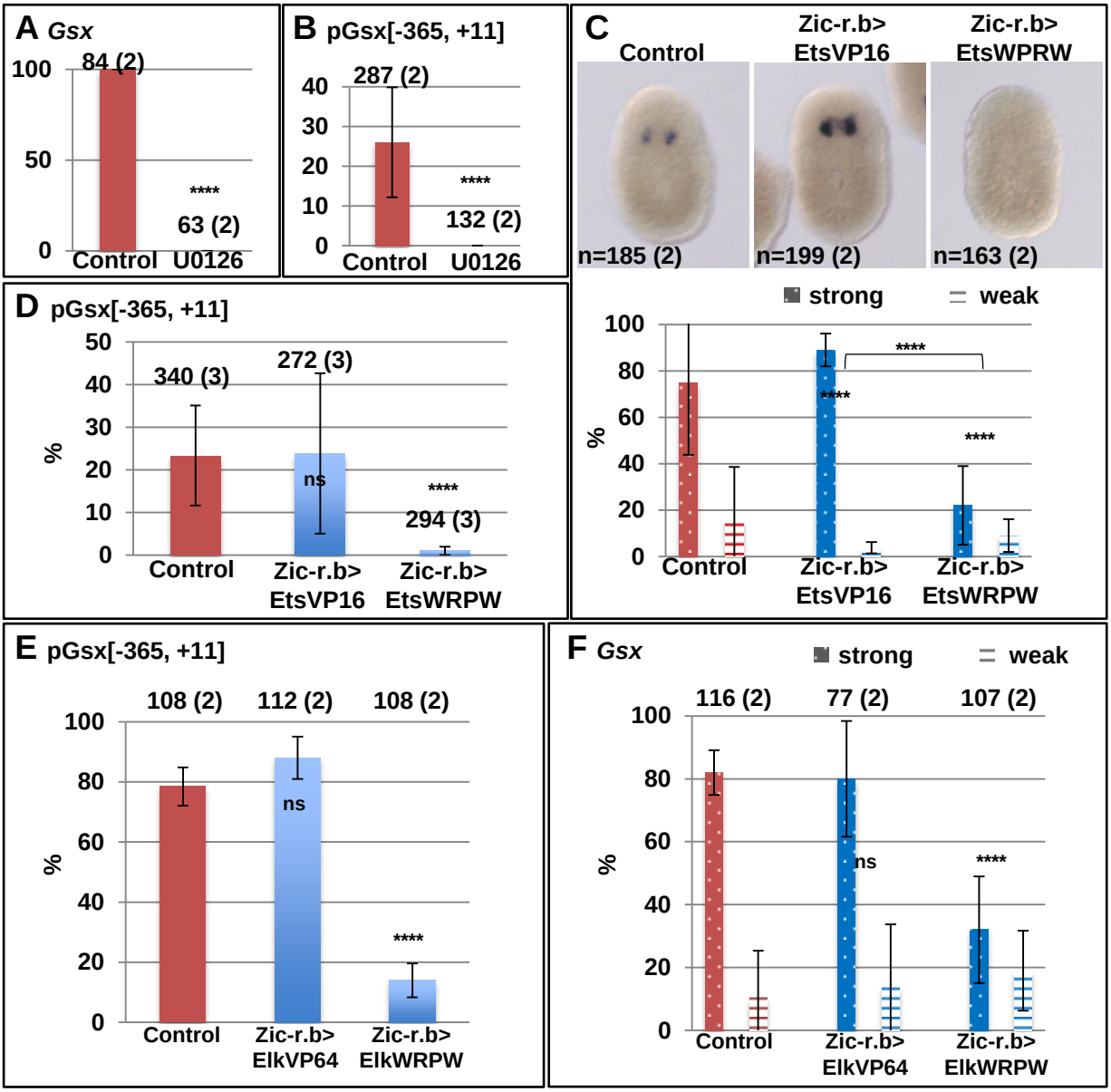
A Gsx
84 (2)
100
50
0
****
63 (2)
Control
U0126
B pGsx[-365, +11]
287 (2)
40
30
20
10
0
****
132 (2)
Control
U0126
C
Control
Zic-r.b> EtsVP16
Zic-r.b> EtsWPRW
n=185 (2)
n=199 (2)
n=163 (2)
strong
weak
100
80
60
40
20
0
%
****
****
****
Control
Zic-r.b> EtsVP16
Zic-r.b> EtsWRPW
D pGsx[-365, +11]
50
40
30
20
10
0
%
340 (3)
272 (3)
ns
****
294 (3)
Control
Zic-r.b> EtsVP16
Zic-r.b> EtsWRPW
E pGsx[-365, +11]
108 (2)
112 (2)
108 (2)
100
80
60
40
20
0
%
ns
****
Control
Zic-r.b> ElkVP64
Zic-r.b> ElkWRPW
F Gsx
strong
weak
116 (2)
77 (2)
107 (2)
100
80
60
40
20
0
%
ns
****
Control
Zic-r.b> ElkVP64
Zic-r.b> ElkWRPW

Figure 4

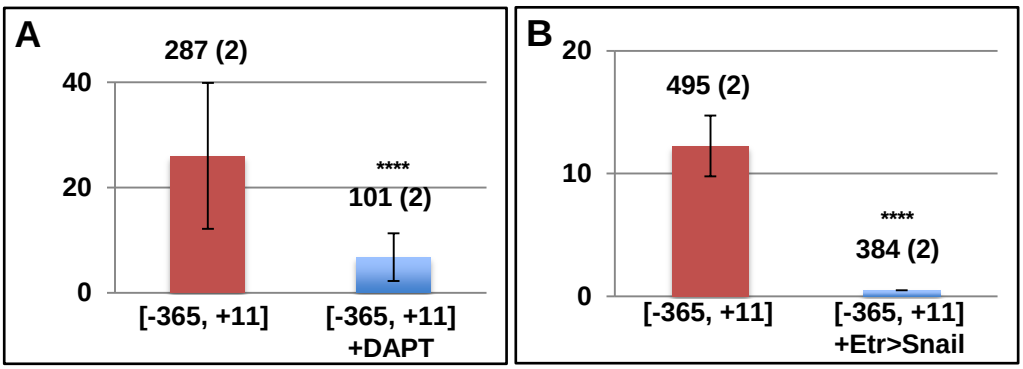
A
287 (2)
40
20
0
****
101 (2)
[-365, +11]
[-365, +11]
+DAPT
B
20
10
0
495 (2)
****
384 (2)
[-365, +11]
[-365, +11]
+Etr>Snail

Figure 5

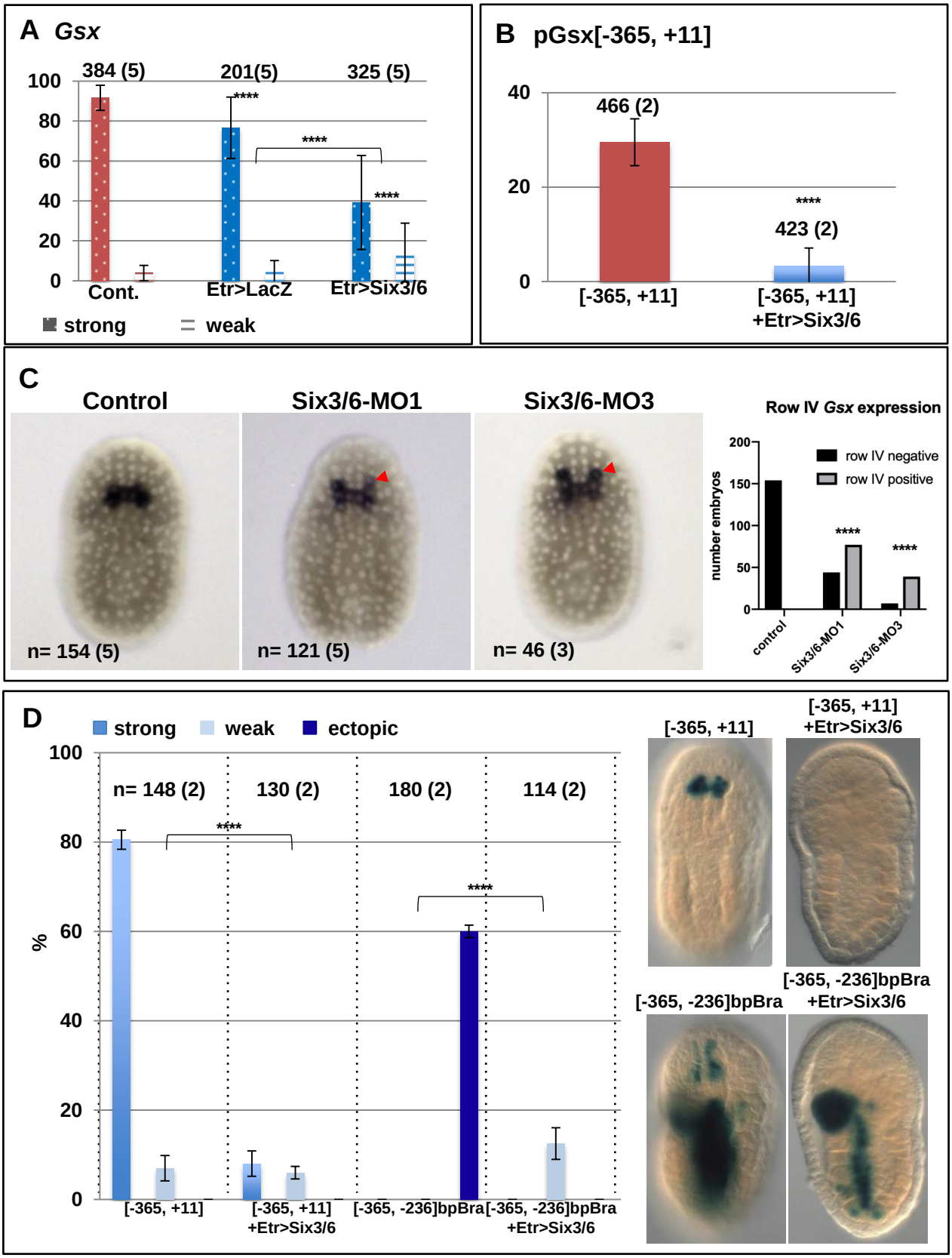
A Gsx
384 (5)
201(5)
325 (5)
100
80
60
40
20
0
****
****
****
Cont.
Etr>LacZ
Etr>Six3/6
strong
weak
B pGsx[-365, +11]
40
20
0
466 (2)
****
423 (2)
[-365, +11]
[-365, +11]
+Etr>Six3/6
C
Control
Six3/6-MO1
Six3/6-MO3
n= 154 (5)
n= 121 (5)
n= 46 (3)
Row IV Gsx expression
number embryos
200
150
100
50
0
row IV negative
row IV positive
****
****
control
Six3/6-MO1
Six3/6-MO3
D
strong
weak
ectopic
100
80
60
40
20
0
%
n= 148 (2)
130 (2)
180 (2)
114 (2)
****
****
[-365, +11]
[-365, +11]
+Etr>Six3/6
[-365, -236]bpBra
[-365, -236]bpBra
+Etr>Six3/6
[-365, +11]
[-365, +11]
+Etr>Six3/6
[-365, -236]bpBra
[-365, -236]bpBra
+Etr>Six3/6

Figure 6

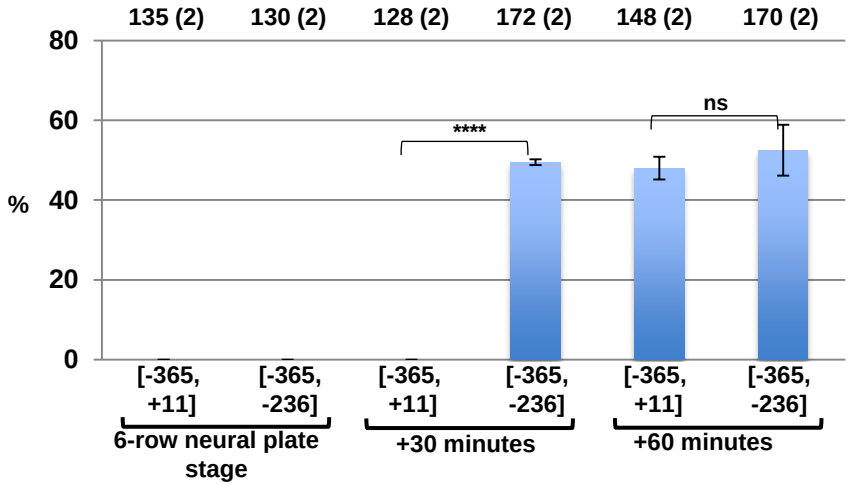

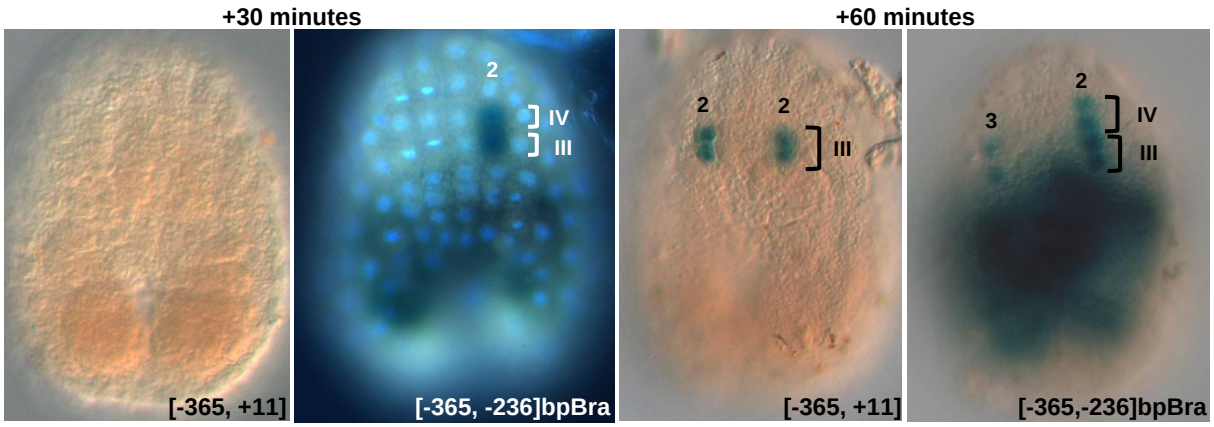

% ectopic activity	-	95	0	86	row IV
	-	46	0	45	column 3

Figure 7

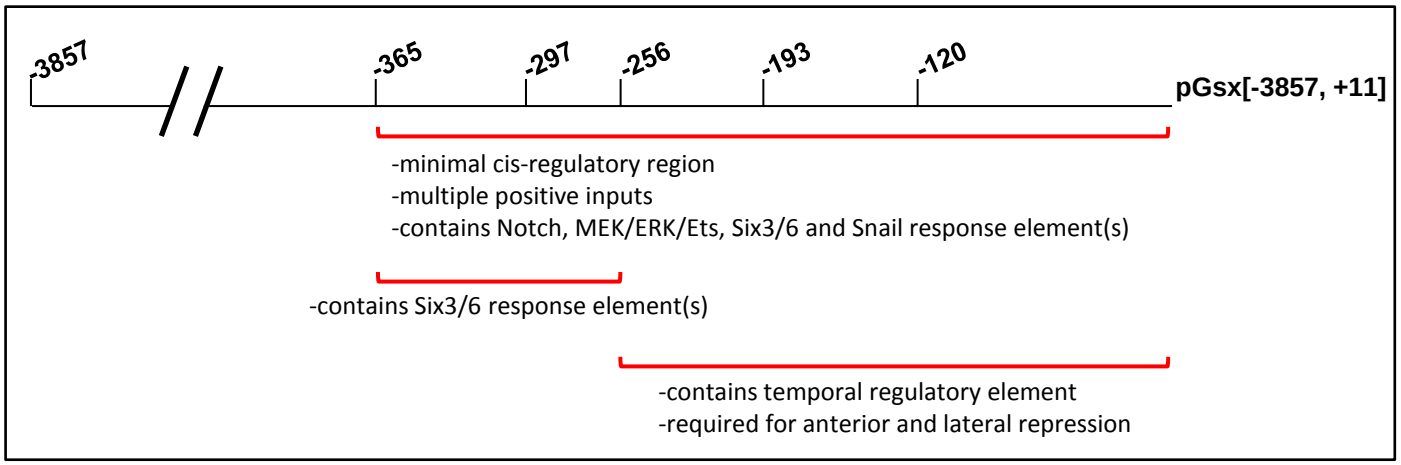
-3857
-365
-297
-256
-193
-120
pGsx[-3857, +11]
-minimal cis-regulatory region
-multiple positive inputs
-contains Notch, MEK/ERK/Ets, Six3/6 and Snail response element(s)
-contains Six3/6 response element(s)
-contains temporal regulatory element
-required for anterior and lateral repression

Figure 8

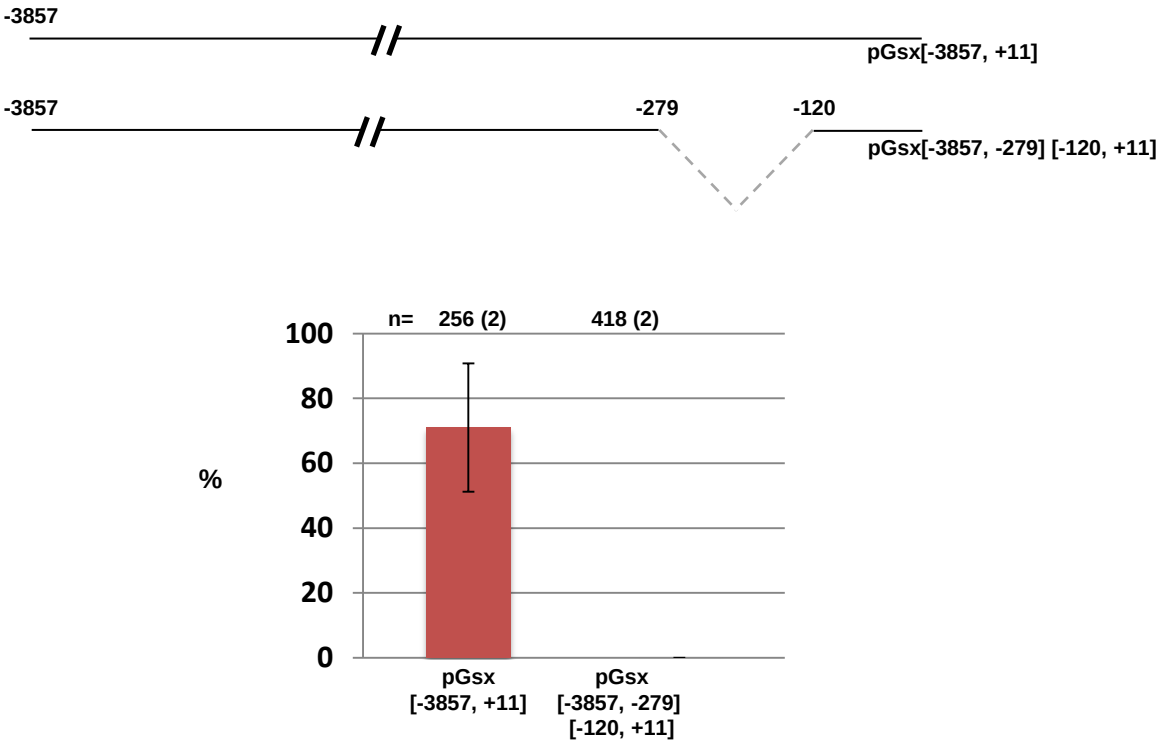

Supplementary Figure 1

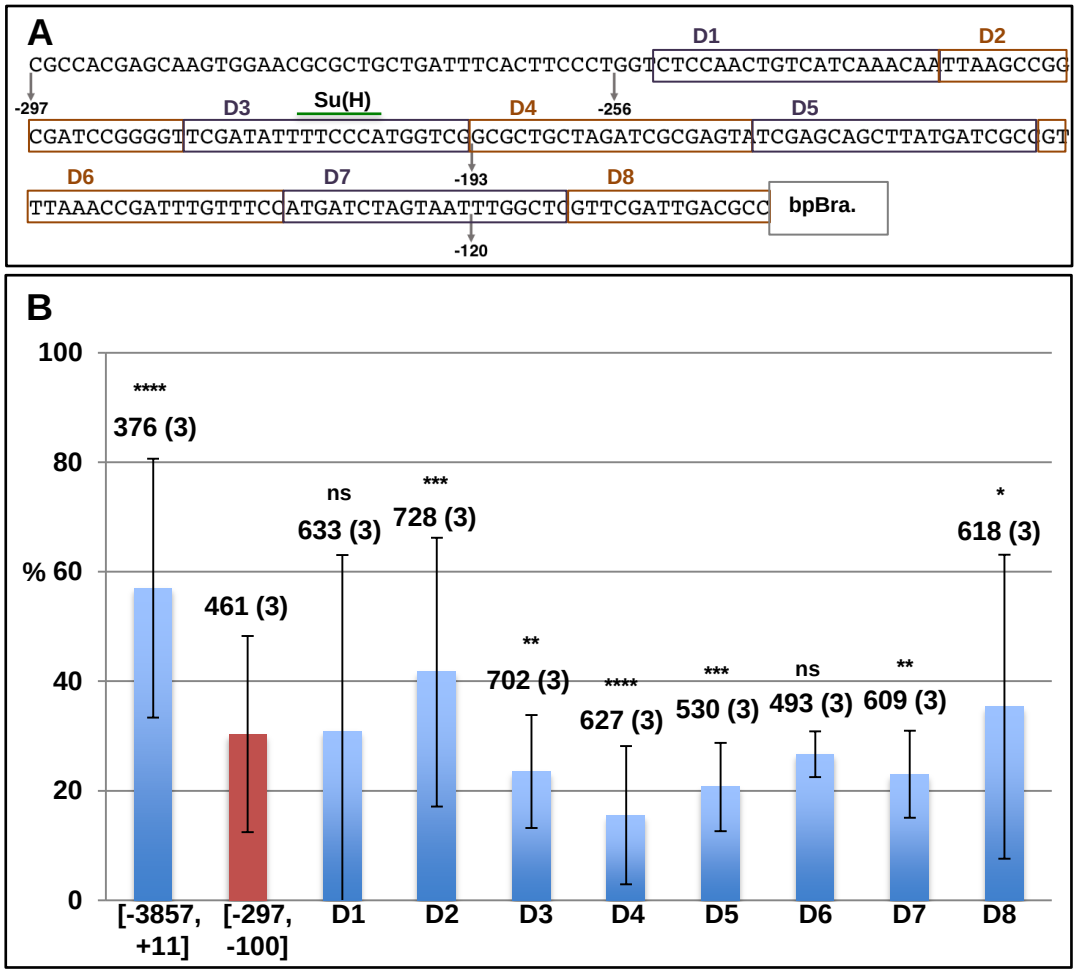

Supplementary Figure 2

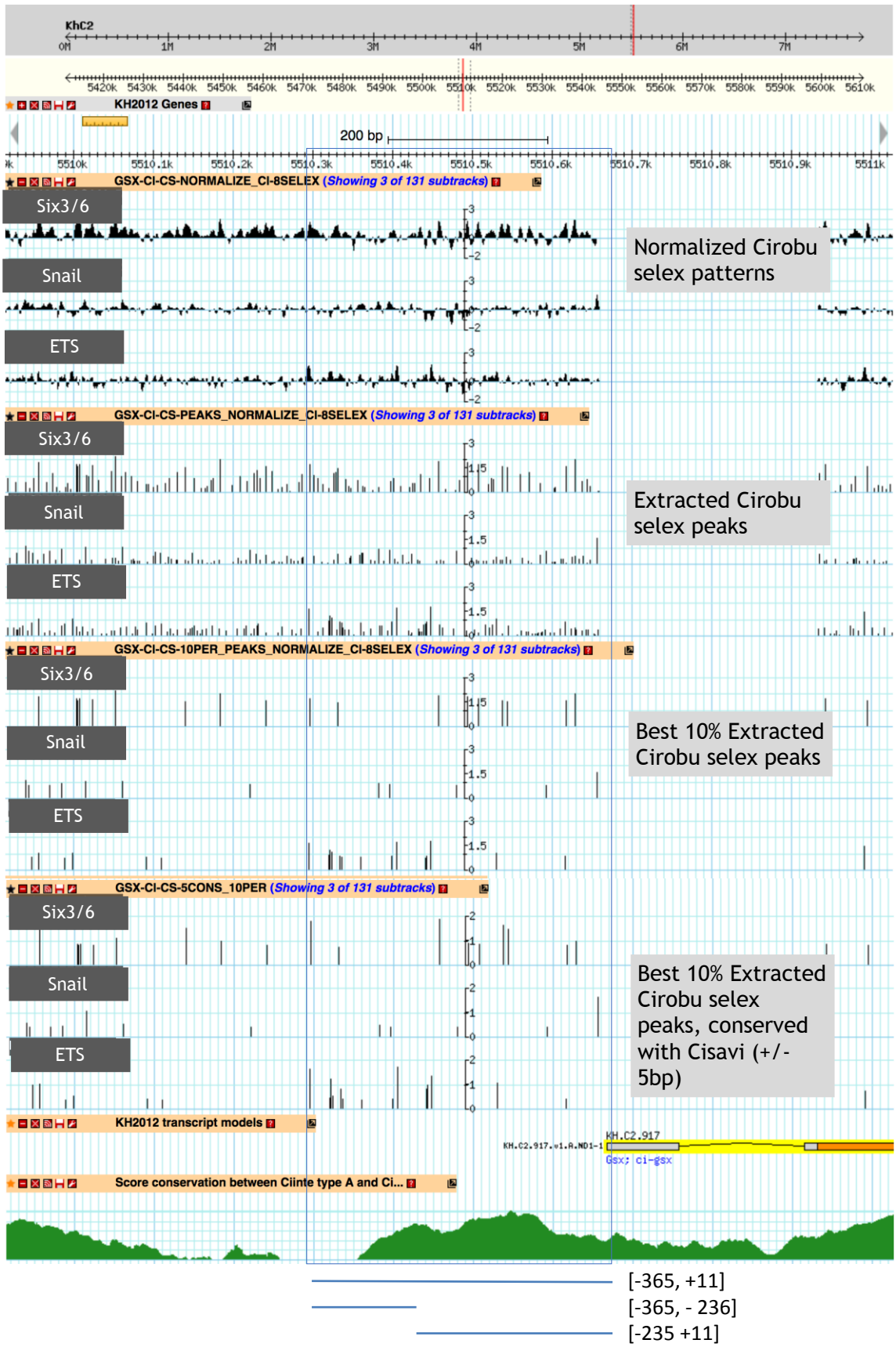

Supplementary Figure 3

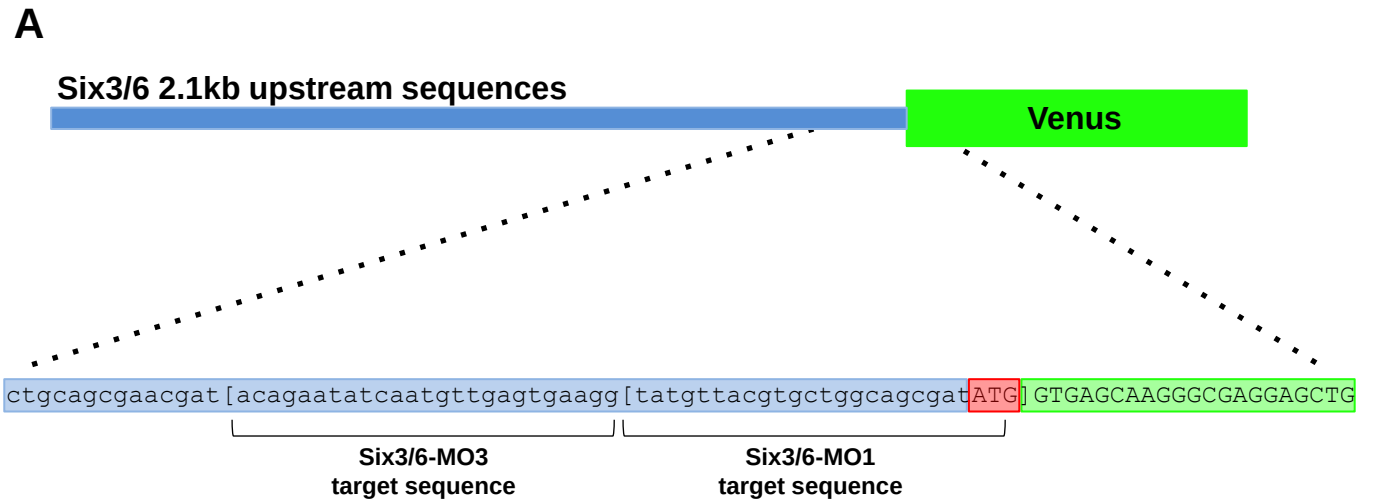

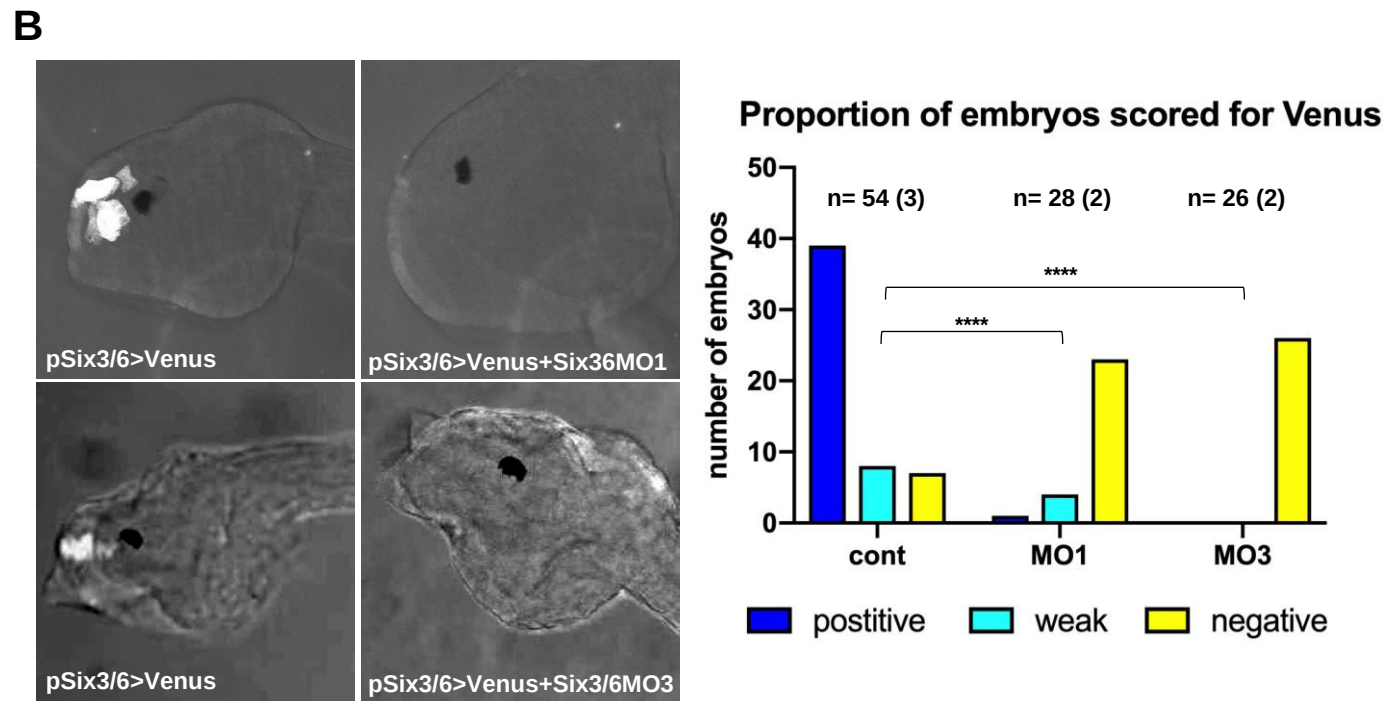

Supplementary Figure 4